Basin Research
IAS EAGE

Clinoform architecture and along-strike variability through an exhumed erosional to accretionary basin margin transition

Journal:	*Basin Research*
Manuscript ID	BRE-132-2018.R1
Manuscript Type:	Original Article
Date Submitted by the Author:	n/a
Complete List of Authors:	Poyatos More, Miquel; University of Oslo, Department of Geosciences Jones, George; Neptune Energy Brunt, Rufus; University of Manchester, School of Earth, Atmospheric and Environmental Sciences Tek, Dan; University of Leeds, School of Earth and Environment Hodgson, David; University of Leeds, Flint, Stephen; University of Manchester, School of Earth, Atmospheric and Environmental Sciences
Keywords:	Clinoform, Shelf-edge, Strike variability, Seabed topography, Inherited basement, sequence stratigraphy, Facies analysis

Clinoform architecture and along-strike variability through an exhumed erosional to accretionary basin margin transition

Poyatos-Moré, M.[1,2]*, Jones, G.D.[3], Brunt, R.L.[2], Tek, D.[4], Hodgson, D.M.[4] and Flint, S.S.[2]

1- Department of Geosciences, University of Oslo, Norway

2- Stratigraphy Group, School of Earth and Environmental Sciences, University of Manchester, UK

3- Neptune Energy, Oslo, Norway

4- Stratigraphy Group, School of Earth and Environment, University of Leeds, UK

*miquel.poyatos-more@geo.uio.no

Abstract

Exhumed basin margin-scale clinothems provide important archives for understanding process interactions and reconstructing the physiography of sedimentary basins. However, studies of coeval shelf through slope to basin-floor deposits are rarely documented, mainly due to outcrop or subsurface dataset limitations. Unit G from the Laingsburg depocentre (Karoo Basin, South Africa) is a rare example of a complete basin margin scale clinothem (>60 km long, 200 m-high), with >10 km of depositional strike control, which allows a quasi-3D study of a preserved shelf-slope-basin floor transition over a ca. 1200 km^2 area. Sand-prone, wave-influenced topset deposits close to the shelf-edge rollover zone can be physically mapped down dip for ca. 10 km as they thicken and transition into heterolithic foreset/slope deposits. These deposits progressively fine and thin over 10s of km farther down dip into sand-starved bottomset/basin floor deposits. Only a few km along strike, the coeval foreset/slope deposits are bypass-dominated with incisional features interpreted as minor slope conduits/gullies. The margin here is steeper, more channelized, and records a stepped profile with evidence of sand-filled intraslope topography, a preserved base-of-slope transition zone and sand-rich

bottomset/basin-floor deposits. Unit G is interpreted as part of a composite depositional sequence that records a change in basin margin style from an underlying incised slope with large sand-rich basin-floor fans to an overlying accretion-dominated shelf with limited sand supply to slope and basin-floor. The change in margin style is accompanied with decreased clinoform height/slope and increased shelf width. This is interpreted to reflect a transition in subsidence style from regional sag, driven by dynamic topography/inherited basement configuration, to early foreland basin flexural loading. Results of this study caution against reconstructing basin margin successions from partial datasets without accounting for temporal and spatial physiographic changes, with potential implications on predictive basin evolution models.

Introduction

Clinothems that build basin margin successions can be subdivided into three physiographic segments: shelf (topset), slope (foreset) and basin floor (bottomset) (Steel and Olsen, 2002; Helland-Hansen and Hampson 2009; Prather *et al.*, 2017). These segments are defined according to the geometry and position of two critical sedimentary transition zones, the shelf-edge rollover (SERZ) and base of slope (BOSZ). These zones are associated with major breaks in clinoform gradient, and their stratigraphic record can provide information on relative sea-level change and sedimentary process interactions (Mutti and Normark, 1987; 1991; Wynn *et al.*, 2002a, b; Steel *et al.*, 2003; Porębski and Steel, 2003; Carvajal and Steel, 2009; Dixon *et al.*, 2012a, b, Jones *et al.*, 2013; Poyatos-Moré *et al.*, 2016; Brooks *et al.*, 2018a). However, the complete stratigraphic record of coeval shelf to basin floor segments along the same clinothem is rarely documented (Pyles and Slatt, 2007; Carvajal and Steel, 2009; Carvajal *et al.*, 2009; Wild *et al.*, 2009; Grundvåg *et al.*, 2014; Prélat *et al.*, 2015; Koo *et al.*, 2016), mainly due to outcrop or subsurface dataset limitations. This limits our understanding of how the interplay of factors, such as pre-existing basin topography, climate, sediment supply, accommodation and dominant process regime, are recorded in different genetically-related positions along a single clinothem profile.

Two-dimensional dip-parallel sections are widely used in clinoform trajectory analysis (Steel and Olsen, 2002; Helland-Hansen and Hampson, 2009, Henriksen *et al.*, 2009), to infer changes in relative sea-level and to predict the timing of coarse-grained sediment delivery to deep water. Clinoform trajectory analysis, however, tends to underplay the role of dominant process regime and along-strike variability in basin margin physiography (Dixon *et al.*, 2012b; Jones *et al.*, 2015), which limits predictability in sediment character and partitioning between the shelf, slope and basin floor segments (Prather *et al.*, 2017; Cosgrove *et al.*, 2018). Modern and subsurface studies demonstrate that along-strike variability in coastal process regime and shelf morphology commonly results in a laterally variable stratigraphic record (Ainsworth *et al.*, 2011; Olariu *et al.*, 2012; Sanchez *et al.,* 2012; Jones *et al.,* 2015; Laugier *et al.,* 2016; Madof *et al.*, 2016), which can also be a key control on the nature of the SERZ (Pyles and Slatt, 2007; Olariu and Steel, 2009; Dixon *et al.*, 2012b; Gomis-Cartesio *et al.*, 2016; Chen *et al.*, 2017). Beyond this zone, the efficient basinward bypass of sediment through the slope is also controlled by seabed topography (Prather *et al.*, 1998; Winker and Booth, 2000; Sinclair and Tomasso, 2002; Smith, 2004a; 2004b; Deptuck *et al.*, 2012; Spychala *et al.*, 2015). Slope gradient and length will control the nature of the BOSZ and the amount and type of sediment that reaches the basin floor (Hubbard *et al.*, 2010; van der Merwe *et al.*, 2014; Hodgson *et al.*, 2016; Prather *et al.*, 2017; Brooks *et al.*, 2018a).

Unit G of the Permian Fort Brown Formation, in the Karoo Basin, South Africa, is a rare outcrop example of an exhumed basin-margin scale clinothem (>60 km long, 200 m-high) with 10 km of along-strike control, which permits extensive analysis of a shelf-slope-basin floor transition. This unit is stratigraphically well constrained by regionally mapped underlying slope-to-basin floor systems and overlying basin margin clinothems. The key objectives for this study are: a) to provide sub-seismic characterization of topset-foreset-bottomset deposits along the same basin margin clinothem; b) to locate the sedimentary transition zones (SERZ and BOSZ) at outcrop and study the facies distribution both down depositional dip and across depositional strike; c) to establish the sequence stratigraphy of a unit deposited during the transition of basin margin style from erosional- to accretionary-dominated; and d) to discuss clinoform depositional pattern variability in time and space, and its wider implications for stratigraphic models of basin margin evolution.

Geological Setting

The Karoo Basin has traditionally been interpreted as a retro-arc foreland basin, developed inboard of the Cape Fold Belt, in response to the northward subduction of the Panthalassan (palaeo-Pacific) plate beneath the Gondwana plate (De Wit and Ransome, 1992; Veevers *et al.*, 1994; López-Gamundí and Rossello, 1998). However, recent radiometric dating (Blewett and Phillips, 2016) and tectonostratigraphic analyses (Tankard *et al.*, 2009; 2012) support a Triassic age for development of the Cape Fold Belt. Subsidence during the Permian pre-foreland basin stage has been attributed to dynamic topography (mantle flow) associated with the subducting plate, with variable foundering of basement blocks (Pysklywec and Mitrovica, 1999; Tankard *et al.*, 2009). A sedimentary source to the SW has been proposed, possibly near the Patagonian Massif (Andersson *et al*., 2004; Van Lente, 2004; Vorster, 2013; Pángaro *et al.*, 2016).

In the Laingsburg depocentre (Fig. 1), the Permian Lower Ecca Group comprises the Prince Albert, Whitehill and Collingham formations, which record an overall deepening of the basin and increasing siliciclastic supply during an icehouse to greenhouse transition (Johnson *et al.*, 2006; Scheffler *et al.*, 2006; Linol *et al.*, 2016). The overlying upper Ecca Group comprises a 1800 m-thick progradational succession from basin-plain deposits (Vischkuil Formation; van der Merwe *et al.*, 2009; 2010; 2011) and basin-floor fans (Units A-B, Laingsburg Formation; Sixsmith *et al.*, 2004; Flint *et al.*, 2011), through a channelized submarine slope (Units C-G; Fort Brown Formation; Grecula *et al.*, 2003; van der Merwe *et al.*, 2014; Brooks *et al.*, 2018b) to shelf-edge and shelf deltas (Waterford Formation; Jones *et al.*, 2015; Poyatos-Moré *et al.*, 2016) (

Fig. 1). Regional palaeoflow is towards the NE and E throughout the succession with the main sediment entry point located to the SW (Flint *et al*., 2011; van der Merwe *et al.*, 2014), although the time-equivalent up-dip depositional systems were eroded during the formation of the Cape Fold Belt. The Ecca Group is conformably overlain by the fluvial/non-marine succession of the Beaufort Group (Rubidge *et al.*, 2000; Gulliford *et al.*, 2014; Wilson *et al.*, 2014).

Dataset and methods

This outcrop study focuses on characterizing Unit G, the youngest unit of the Fort Brown Formation, and its relationships with its underlying and overlying stratigraphy. Unit G is exposed along the limbs of post-depositional folds with W-E trending axes in the Laingsburg depocentre, across a ca. 1200 km^2 area (

Fig. 1). The stratigraphic position of Unit G is well constrained by regionally mapped underlying deep-water slope to basin-floor systems and overlying shelf and deltaic deposits (Fig. 2). The fieldwork dataset includes 23 detailed sections measured at cm-scale to characterize the range of sedimentary facies and facies associations (Table 1), supported by 152 thickness logs for Unit G from previous work (

Fig. 1) (Figueiredo *et al*., 2010; Flint *et al*., 2011; van der Merwe *et al*., 2014; Jones *et al*., 2015). A correlation framework established by walking out stratigraphic surfaces between sections was used to build thickness and facies maps over tens of kilometres in depositional dip and strike. Thickness distribution maps were created by fitting a surface to values obtained from logged sections using the kriging tool within the ArcGIS® Geostatistical Wizard. By combining these maps with sedimentary and stratigraphic information, a palaeogeographic reconstruction representing the gross depositional environments of Unit G was built. This is further complemented by restored palaeocurrent data from 236 measurements of cross-bedding foresets, ripple cross-lamination, primary current lineation, basal tool marks and erosion surface orientations. These data are also supported by c. 50 km of oblique helicopter-based and UAV photography.

Facies and facies associations

Table 1 summarizes a process-based facies scheme, which includes 21 lithofacies, with a description and interpretation of lithology, grain size, sedimentary structures, bed thickness and boundaries and geometries. These lithofacies stack in different facies associations (Table 2), which are used to characterize architectural elements and their interpreted environments of deposition. Because of its stratigraphic position, Unit G includes both shallow and deep water facies associations.

Map data

Palaeocurrent analysis

Figure 3A shows palaeocurrent data for Unit G. Most of the unidirectional data are consistent with the long term depositional dip direction to the E and ENE in underlying (Flint *et al.*, 2011; van der Merwe *et al.,* 2014) and overlying (Jones *et al.*, 2015; Poyatos-Moré *et al.*, 2016) strata. The spread of current directions is higher in the most proximal south-western exposures, and is related to either multiple sediment entry points or redistribution processes. The bidirectional data are from symmetrical ripples restricted to the SW of the study area, and have a NE-SW azimuth, which is consistent with a NW-SE orientation of the basin margin, almost perpendicular to the orientation of wave reworking.

Thickness analysis

Figures 3B, C and D show the thickness distribution of the stratigraphic package between top Unit F and base Unit G (Fig. 3B), Unit G (Fig. 3C), and from top Unit G to the top of the second shallow marine parasequence (WfC 2) of the Waterford Formation (Fig. 3D; Jones *et al.*, 2013; 2015). These packages were chosen to be plotted due to their good stratigraphic control, and because they show thickness information from below and above Unit G.

The mudstone-dominated package between top Unit F and base Unit G shows a relatively constant basinward (eastward) thinning (ca. 120-20 m; Fig. 3B). The overall wedge-shaped thickness distribution of this package is taken to record the slope physiography prior to deposition of Unit G. The thickness map of Unit G shows an initial abrupt eastward thickening (only seen in the SW) followed by an overall thinning trend that is disrupted in the central northern area by a "thick" (Fig. 3C). This thicker area is located slightly up-dip of a N-S oriented thick in the underlying Unit F to G mudstone (Fig. 3B). The mudstone-dominated package between top Unit G and top WfC 2 shows an eastward thickening in the westerly up-dip area (Fig. 3D), to a thickness maximum of ca. 180 m, followed by an eastward (basinward) thinning.

The basinward thickening-then-thinning pattern observed in both Unit G and the mudstone package between Unit G and WfC 2 is evidence of two clinothem topset-foreset-bottomset geometries, with the inferred location of the respective clinoform rollover zones landward of the thickness maximum. The mudstone thickness maps (Fig. 3B, 3D) also provide evidence for the progradation of successive, mud-dominated clinothems between Unit F and WfC 2. This is evidenced by the location of the clinoform rollover, which in Unit G is to the SW of the study area, whereas by WfC 2 time the shelf had prograded by at least 20 km.

Architecture and facies distribution of Unit G

The stratigraphic architecture of Unit G is reconstructed using three depositional dip-orientated correlation panels, from south (A) to north (C; Fig. 4), which also illustrate the depositional strike variability. Previous work in the underlying/overlying stratigraphy has established recognition criteria to place each studied section within a basin margin position based on geometry, depositional architecture, sedimentary processes and resulting deposits (*e.g.* Jones *et al.*, 2013;

Brooks *et al.*, 2018a). These criteria are combined here with the map data and used to divide Unit G into three spatial segments: proximal (topset), intermediate (foreset) and distal (bottomset), separated by the shelf-edge rollover (SERZ) and base-of-slope (BOSZ) zones. A similar topset-foreset-bottomset nomenclature has been employed for clinothems of similar scale that developed above deep shelves (*e.g.*, Anell *et al.*, 2014; Patruno *et al.*, 2015; Hodgson *et al.*, 2018; Pellegrini *et al.*, 2018) or in lakes (*e.g.*, Fongngern *et al.*, 2016; 2018), and are also comparable in scale to other systems where topsets are referred to as the shelf, foresets as the slope, and bottomsets as the basin floor (*e.g.*, Carvajal *et al.*, 2009).

Proximal (topset) segment

Description

Between the BS1 and BS3 localities in the SW of the study area (Figs. 1, 4) Unit G is separated by ca. 100 m of regional mudstone (Fa1 facies, Table 1) from the underlying Unit F. Here, Unit G is 32 m-thick and is overlain by a regional ca. 30 m-thick mudstone package and the distal prodelta facies of the lowermost deltaic parasequence (WfC 1, Jones *et al.*, 2015). Unit G is divided into three sub-units (G1, G2, G3; Fig. 5) each of which is topped by m-thick fine siltstone-dominated sections of regional extent (Fa2). In the BS2 locality, sub-unit G1 comprises a 2 m-thick, upward coarsening, heterolithic package (Fa4 to Fa5) that is cut by a shallow, sandstone-filled erosion surface that can be mapped for several hundreds of metres before it pinches out to the east of BS1 and to the west of BS3. The surface is overlain by a mudstone clast conglomerate (Fa17; Fig. 5), and the fill comprises very fine- to fine-grained structureless sandstone (Fa6), cross-bedded sandstone (Fa7), and mud-clast rich horizons (Fa17). An overlying 8 m-thick fining- and thinning-upward section of thin beds (Fa5 to Fa4) is capped by a 0.5 m siltstone (Fa2).

The base of sub-unit G2 is marked by a 0.4 m-thick poorly sorted muddy sandstone bed (Fa21) (Fig. 5). The overlying succession comprises heterolithic deposits (Fa4, Fa5), abruptly overlain by a 2 m-thick coarsening- and thickening-upward package characterised by several 5-15 cm-thick sandstone beds with hummocky cross stratification (Fa13). The upper two thirds of sub-unit G2 comprise ca. 10 m of fining- and thinning-upward thin beds (Fa5 to Fa4) with wave-modified current-ripple-laminated sandstones (Fa12) punctuated by 10 cm-thick climbing ripple laminated sandstone beds (Fa14). Sub-unit G2 is capped by a regionally mapped siltstone (Fa2) (Fig. 5).

Sub-unit G3 in the BS1 to BS3 localities is marked by an overall increase in grain size, bed thickness and amalgamation, and sandstone content (Fig. 5). Sandstones are poorly sorted and have a characteristic light brown colour, with common mud-filled burrows. G3 sandstones have poorly preserved bedding and generally lack primary sedimentary structures. The top of sub-unit G3 in this proximal setting is marked by an abrupt transition into the overlying mudstone (Fa1) (Fig. 5), and is characterized by abundant vertical burrowing and reddish staining.

Interpretation

The presence of incision surfaces at the base of Unit G mantled by mudstone clast conglomerates (Fig. 5B) is consistent with several phases of erosion and sediment-bypass, forming a lag deposit. The overlying fining- and thinning-upward heterolithic section of sub-unit G1 (Fig. 5A) either represents a landward stepping due to transgression and increased accommodation, or the final infill of a deeper incision (see Gomis-Cartesio *et al.*, 2018). The presence of hummocky-cross stratification in sub-unit G2 (Fig. 5C) indicates deposition above storm wave base and the absence of sediment bypass indicators suggests a setting that transitioned from bypass to accretion-dominated. The regional siltstone capping sub-unit G2 is interpreted as containing a flooding surface (Fig. 5A, ca. 25 m). Sub-unit G3 is interpreted as progradational, sand-prone, wave/storm-influenced distal mouth bar/lower shoreface deposits. Here, Unit G is interpreted as deposited in a shallow-marine shelf/topset setting (Fig. 5D), representing the most proximal facies observed. The highly bioturbated top of Unit G is interpreted to mark a major transgression and deepening prior to deposition of a thick hemipelagic mudstone unit (Figs. 2, 5D).

Intermediate (upper foreset) segment – southern area

Description

Down-dip (eastward) of locality BS3, there is a pronounced facies change, and Unit G is much thicker here than in the more up-dip exposures (Figs. 3C, 4A). Facies are typified by the BN2 locality, where Unit G is 27 m-thick, and has an overall symmetrical vertical profile (coarsening- and thickening- then fining- and thinning-upward, Fig. 6F) with two internal siltstones that mark the subdivision into G1, G2 and G3 (Fig. 6E). The base of sub-unit G1 is marked by a 0.3 m-thick laminated siltstone (Fa2, Table 1) overlain by a sharp-topped 2.5 m-thick, heterolithic coarsening- and thickening-upward package (Fa4 to Fa5) dominated by 2-5 cm-thick unidirectional ripple-laminated silty sandstone beds (Fa11). A 1 m-thick laminated siltstone (Fa2) and a muddy unit with siderite concretions (Fa1) separates sub-unit G1 and G2. The lower 6 m of sub-unit G2 coarsens- and thickens-upward and comprises heterolithic deposits (Fa5) and unidirectional ripple laminated sandstones (Fa11), overlain by thicker climbing ripple dominated sandstones (Fa14) (Fig. 6A). The top of sub-unit G2 is sharp and overlain by a 0.4 m-thick laminated siltstone (Fa2) with a basal concretion-rich horizon (Fa1). Sub-unit G3 (22 m-thick) consists of fining- and thinning-upward thin bedded, unidirectional ripple and stoss-side preserved climbing ripple-laminated sandstones and siltstones (Fa5, Fa11, Fa14, Fig. 6G). Thicker beds (5–10 cm-thick) have a characteristic inverse to normal grading (Fa9). The lower inverse graded division is cut and overlain by a strongly unidirectional or climbing ripple laminated coarse-grained sandstone that fines and thins upward into a capping bioturbated siltstone (Fa2) (Fig. 6H).

Interpretation

The coarsening- and thickening- then fining- and thinning-upward trend of Unit G is interpreted to represent progradation followed by retrogradation of the system (Fig. 6E). The significant thickening combined from the west of this location with a change from an asymmetric to a more symmetrical profile are consistent with a basinward increase in accommodation. The intensive basal scouring and erosion in the more proximal (west) localities is no longer present and Unit G in intermediate localities has a more accretionary style of deposition. These changes are interpreted to be consistent with a position close to the shelf-edge, and are also associated with a change in the dominant process regime. The presence of lenticular bedded sandstones with strong unidirectional, climbing and stoss-side preserved ripple lamination and the absence of wave reworking (symmetrical ripples, HCS and SCS) suggests rapid deceleration of flows escaping confinement or expanding onto an upper slope setting, below storm wave base. The "composite" internal architecture of many of the beds (Fig. 6A) (inverse to normal grading and internal erosional surfaces) is considered to represent frequent sediment bypass and a potential direct linkage to the fluvial feeder system, and are therefore interpreted as hyperpycnal flow deposits (Mulder *et al.*, 2003; Plink-Björklund and Steel., 2004; Bhattacharya and MacEachern, 2009; Zavala *et al.*, 2011, Dixon *et al.*, 2012a).

Intermediate (upper foreset) segment – northern areas

Description

Intermediate localities of Unit G in the north of the study area (Figs. 4C, 6A) retain a similar threefold internal sub-division, and the overall coarsening- and thickening-upward then fining- then thinning-upward profile. The FB2 log represents the type locality for the intermediate northern area (Fig. 6A). Sub-unit G1 here is characterized by a 2-m thick coarsening- and thickening-upward package of heterolithic thin beds (Fa4 to Fa5, Table 1), cut by small sandstone-filled erosive features up to 3 m-wide and 0.5 m-deep. This is overlain by a section of sigmoidal bedded sandstones (4 m-thick, Fig. 6C) with stoss-side preserved climbing ripple lamination (Fa15), capped by a 2 m-thick package of heterolithic thin beds (Fa5) and a 1 m-thick siltstone with siderite concretions (Fa1), which marks the boundary between sub-unit G1 and G2 (Fig. 6A).

The base of sub-unit G2 is marked by two 2 m-thick fining- and thinning-upward heterolithic packages (Fa5 to Fa4), which are overlain by a 13 m-thick coarsening- and thickening-upward section of heterolithic (Fa5) and thin bedded sandstones dominated by unidirectional ripple lamination (Fa11). Sub-unit G2 is capped by a 0.5 m-thick folded unit (Fa19), and a 2 m-thick laminated siltstone (Fa2). Sub-unit G3 comprises a lower coarsening- and thickening-upward heterolithic package (Fa4 to Fa5; 3 m-thick) overlain by a 2 m-thick deformed deposit comprising undulating and contorted heterolithic facies (Fa19), and a 13 m-thick upper section that fines- and thins-upward into the overlying mudstone (Fa2).

Exposures along the Zoutkloof/Faberskraal panel (Figs. 1, 4C) indicate that Unit G thins markedly over 18 km from its thickest position at FB1 (Zoutkloof River; 85 m-thick) to the FB5 locality (6 m-thick; Figs. 3C, 4C). The three-part division, as seen in Fig. 6E, is identified at most localities. Elsewhere in the western localities, sub-unit G1 is characterized by sigmoidal sandstone beds with internal stoss-side preserved climbing ripple laminations (Fa15). Typically, the basal surface of Unit G is gradational from the underlying mudstone (Fig. 6A). However, in the FB4 log the base is marked by small, sand-filled erosive scours (Fa16, Fig. 6B) that cut into the underlying mudstone (Fa1). These erosive features are sharp-topped, highly discontinuous and pinch out abruptly (laterally) into background mudstone.

Interpretation

Unit G in the north of the study area displays an overall similar symmetrical vertical profile to the south, but it shows major differences in both thickness trends and facies (Fig. 4C). The lower part (sub-unit G1) is dominated by interbedded, strongly unidirectional, stoss-side preserved climbing ripple-laminated sandstone (Fa14 and Fa15). Deposits show no evidence for wave reworking, which suggests rapid deposition of unconfined flows below storm wave base, consistent with an upper slope setting. The stoss-side preserved climbing ripple lamination observed in sub-unit G1 is similar to that described for external levee facies in the underlying deep water slope units (Morris *et al.*, 2014). The presence of erosive features around the FB4 locality are also consistent with local sediment bypass and gullying. The westernmost exposures of Unit G in the northern areas show an upper slope system dominated by instability and mass-wasting processes, with debrites infilling erosion surfaces, slump scars and associated deformed strata. These coupled with the relatively more abrupt thickness decrease point towards the presence of a steeper, northern margin.

Intermediate (lower foreset) segment

Description

In the south, Unit G has been mapped for 40 km along the Baviaans South Panel (Fig. 1), where it thins down depositional dip from 63 m (BS4) to <1m in the most distal locality (BS8) (Fig. 4A). On the Baviaans North Panel (Fig. 1), Unit G can be also correlated for about 35 km down dip, where it thins from 48 m (BN1) to 3 m (BN5) (Fig. 4B). However, in the north of the study area, Unit G does not display a simple basinward thinning. From a maximum thickness of 85 m in FB1, it thins to 6 m over a dip length of 20 km at the FB5 locality, where it comprises only two heterolithic packages separated by a 0.45 m-thick intra-unit mudstone (Fig. 4C). Basinward of this position (FB6), the base of Unit G is marked by a 10 m-thick, erosive-based amalgamated sandstone-dominated package (Fig. 7), which comprises structureless, normally-graded fine to medium-grained sandstones (Fa6 and Fa8) (Fig. 7A). Numerous erosion surfaces mantled with mudstone clasts (Fa17) (Fig. 7C, D) cut down into the underlying mudstone with a relief of up to 5 m (Fig. 7C). Flute marks are common and indicate E- to NE-directed flows (Fig. 3A). The top of the lower sand-dominated section is characterized by an abrupt transition into 1 m-thick laminated siltstone dominated facies (Fa3) cut by up to 0.3 m-deep sandstone-filled erosive scours (Fa16) (Fig. 7E). This laminated siltstone is overlain by a 13 m-thick coarsening- and thickening-upward package of heterolithic facies (Fa4 to Fa5), which fines- and thins-upward abruptly into the overlying mudstone (Fa1) (Fig. 7A). Lack of exposure between FB5, where the three subdivisions of Unit G are still clearly visible, and FB6 precludes the correlation of internal divisions (Fig. 4C). Therefore, the relationship between the amalgamated sandstone unit and the up-dip heterolithic subdivisions of Unit G observed at FB5 remains poorly constrained. The lower sandstone-dominated package is mappable for ca. 1.5 km down dip (east), where it thins abruptly. Farther east, Unit G is only represented by a siltstone-dominated interbedded package (Fa4) in the FB7 locality (Fig. 4C).

Interpretation

The overall coarsening-upward profile of Unit G in distal localities is interpreted as the fine-grained expression of a lower clinothem foreset in a slope setting. However, in the Faberskraal-Zoutkloof profile (Fig. 4C), the m-scale erosive-based fine to medium-grained sandstone packages with mudstone clast-rich horizons at the base of Unit G shows evidence of recurrent sediment bypass. These lower erosive beds are sharp-topped, highly discontinuous and tend to pass abruptly into the background siltstone-dominated sediments (Fig. 7E). They are interpreted as sand-rich intraslope deposits in a bypass dominated part of the slope (Spychala *et al.*, 2015; Brooks *et al.*, 2018b), and are overlain by heterolithic lower foreset deposits of sub-unit G3.

Distal (bottomset) segment

Description

Unit G in distal settings is usually characterized by a thin coarsening- and thickening-upward package of siltstone-prone bioturbated thin beds (Fa4), which fine and thin down dip into the mudstone-dominated background sedimentation (Fa1). However, in the easternmost (most distal) locality in the northern Zoutkloof/Faberskraal panel (FB8, Fig. 4C), Unit G shows an abrupt basal transition from the underlying mudstones (Fa1) into a ca. 10 m thick sandstone-dominated package (Fig. 8). Commonly, this sharp and erosive contact is accompanied by underlying discordant sandstones with lineations on top and base surfaces, interpreted as clastic injectites (Fa18; see Cobain *et al.,* 2015) (Fig. 8B, C). The basal sandstone package is composed of several discrete erosive-based, clean and structureless fine-grained sandstone beds (Fa6), with a sub-tabular geometry (although with common erosional and/or amalgamation surfaces), interbedded with muddy debrites (Fa20) and hybrid event beds (Fa21) (Fig. 8D). They are abruptly overlain by a silt-rich, heterolithic and moderately bioturbated upper package (Fa4) (Fig. 8A).

Interpretation

The progressive down dip thinning of Unit G towards the eastern part of the Zoutkloof/Faberskraal syncline suggests a lower foreset-to-bottomset geometry. This thickness trend combined with the sandstone-dominated deposits at the FB8 locality is interpreted to represent proximal basin-floor lobe deposits at the clinoform base-of-slope. Their relatively sharp tops may suggest avulsion-driven lobe abandonment (Prélat and Hodgson, 2013), or sediment bypass (Stevenson *et al.*, 2015). The overlying siltstone-prone thin beds are interpreted as the distal clinoform toes of the upper coarsening and thickening-upward subunits of Unit G, better developed in positions upslope. Injectites are commonly associated with abrupt up-dip pinchouts in basin-floor settings (Cobain *et al.*, 2017).

Palaeogeography of Unit G

Integration of thickness patterns, palaeocurrent trends and facies distributions constrain the palaeogeographic configuration of Unit G (Fig. 9). The location of the shelf-edge in Unit G separates the gullied shallow marine topset facies exposed between BS1 to BS3 (Figs. 4, 5) from the hyperpycnal foreset deposits of BN2/BS4 (Figs. 4, 6). Unit G is predominantly composed of heterolithic prodelta deposits distributed along a NW-SE trending shelf-edge rollover zone (Fig. 3C), with wave-reworked shelf/topset distal shoreface deposits in the south-western corner of the Laingsburg depocentre (Fig. 9). In the foreset segment, Unit G shows a significant strike variability, with a simple basinward clinoform thinning in the south (Fig. 4A) and a more complex configuration in the north (Fig. 4C). Here, slumps and erosional features are present in the west (up-dip), and two 'thicks' (Fig. 3C) coincide with basal sandstone packages in the FB6 and FB8 localities (Figs. 4C, 7, 8). The thickening of Unit G at FB6 is coincident with a zone of thinning of the mudstone package between top Unit F and base Unit G (Fig. 3C), suggesting that underlying seabed topography played a significant role in the location of intraslope sandstone-dominated packages, as also described for the underlying units (Spychala *et al.*, 2015; Brooks *et al.*, 2018b). The abrupt top of the intraslope sandstone body suggests that the feeder system might have abruptly propagated basinward lateral to this area when the available accommodation was filled, to feed a proximal basin-floor fan beyond the base-of-slope near the FB8 locality (Figs. 4C, 8).

Discussion

Basin-fill evolution

A regional-scale dip-parallel correlation panel (2 km-thick, 50 km-long) flattened on the top of Waterford parasequence WfC8 of Jones *et al.* (2015), shows the stratigraphic architecture of the Laingsburg depocentre succession (Fig. 10A), and highlights the asymmetric geometry of the basin-fill. Above the basal Collingham Formation, which has a constant thickness at the scale of the depocentre (Viljoen, 1994), interbedded basinal mudstone and mass-transport deposits of the Vischkuil Formation show a constant eastward (basinward) decrease in overall thickness, from 380 to 150 m (van der Merwe *et al.*, 2009). This thinning trend is also present in the overlying sandstone-rich basin floor fan deposits of Units A and B, accompanied by a progressive down dip facies change from proximal (west) to distal (east) (Grecula *et al.*, 2003; Sixsmith *et al.*, 2004; Flint *et al.*, 2011; Brunt *et al.*, 2013a, b). The overlying slope deposits of Units C to F also thin towards the east from slope valley-fills through channel-levee deposits to basin floor lobe complexes (Grecula *et al.*, 2003; Flint *et al.*, 2011; van der Merwe *et al.*, 2014). Over time the slope system progressed from the progradational sand-attached systems of Units C and D to relatively fixed sand-detached systems with well-preserved channel-lobe transition zones in Units E and F (van der Merwe *et al.*, 2014; Brooks *et al.*, 2018a). The regional mudstone-rich packages between the deep-water units also thin basinward, resulting in a marked wedge-shaped geometry (Fig. 10A). Thus, the Vischkuil Formation to Unit F succession shows a persistent area of sediment accumulation in the western part of the Laingsburg depocentre through time, which influenced sediment distribution through the continued generation of subtle seabed topography during deposition of the deep water units (Brooks *et al.*, 2018b, see also Fig. 3B).

Unit G itself marks a major transition in the stratigraphic arrangement of the basin fill. The mudstone package between units F and G is the youngest unit to record a thicker accumulation in the western part of the depocentre (Fig. 3D), although its wedge geometry is more pronounced than in the underlying units, with eastward thinning from >100 m to a few tens of metres over <50 km (Fig. 3D, 10B). Above this, Unit G displays an overall basinward thickening then thinning clinothem geometry from proximal (west) to distal (east), punctuated by local sand-filled intraslope topography in the north (Figs. 3C, 4C, 9). The younger mudstone package that separates Unit G from the overlying stratigraphy records a clear eastward step in its thickest development (Fig. 3B) and is overlain by the progradationally stacked seaward-dipping WfC1-8 clinothems of the Waterford Formation (Jones *et al.*, 2015; Fig. 10B). Differential thickness distribution of Unit G across strike, with more accommodation towards the northern part of the depocentre (Fig. 3C), is a possible control on the overall steeper gradient and increased sediment bypass, as has also been reported in the overlying Waterford Formation parasequences (Jones *et al.*, 2015).

Linking deep- and shallow-water sequences

Using the same criteria as for earlier studies on underlying units E and F (Flint *et al.,* 2011), the presence of two regional internal fine siltstones suggest that Unit G can be interpreted as a lowstand sequence set comprising 3 internal depositional sequences, which can be identified in most locations (Fig. 4). At a larger scale, Unit G, the regional overlying mudstone and the lower part of the Waterford Formation are interpreted as a composite sequence set (Flint *et al.*, 2011; Jones *et al.*, 2015).

Internally, depositional sequences within Unit G preserve sandy highstand shelf deposits in the southern up-dip area, with slope thin-beds and overall basin floor lowstand fine-grained deposits. However, the widespread evidence for erosion and indicators of sediment bypass in the shelf segment suggest limited accommodation conditions. Along strike to the north, where the coeval foreset to bottomset stratigraphy of the clinothem is exposed, Unit G exhibits sand-rich lowstand deposits, either healing intraslope topography or beyond the clinoform base-of-slope. This lateral variability in the expression of systems tracts and nature of bounding surfaces has been highlighted in other studies (e.g., Martinsen and Helland-Hansen, 1995; Burgess and Prince, 2015), but rarely documented in exhumed clinothem successions (e.g. Laugier and Plink-Björklund, 2016). In the Karoo Basin margin succession, this along-strike variability is inherited from the underlying units, persists through the whole deep-water stratigraphy (Brooks *et al.*, 2018b) and is also observed in overlying shelf units (Jones *et al.,* 2015). This variability has different expressions and controls in different depositional environments. In the underlying deep-water section, it marked by the south to north switch of the main feeder system, between Unit D and Unit E (Figueiredo *et al.*, 2010). In Unit G, the variability is expressed in terms of slope gradient and morphology, with intraslope lobes and basin-floor fan deposits restricted to the north (Figs. 4C, 9). In the overlying shelf deposits, the along-strike variability is marked by changes in the dominant process regime, with more river-dominated deltas to the north and lateral variability in rate of progradation, shelf width and distribution of sand on the upper slope (Jones *et al.*, 2015).

Unit G marks a change in the arrangement of depositional sequences within the basin-fill (Fig. 11A). In the deep-water succession, depositional sequences are characterised by mappable erosional sequence boundaries on the slope and thick sand-prone LST deposits on the basin-floor, overlain by a thin and muddy combined TST/HST (Flint *et al.*, 2011). These depositional sequences underlying Unit G contrast with the almost absent LST, thin TST and thick HST dominated sequences in the overlying Waterford Formation, together with the absence of evidence for subaerial exposure, shelf-incised valley-fills, or clear sequence boundaries (Jones *et al.,* 2013, 2015) (Fig. 11B). HST deposits in deep-marine sequences are recorded by sand-poor interfan mudstones, suggesting absence of significant sand delivery or that sufficient shelf accommodation must have existed to sequester most of the sand component (*e.g.*, Porębski and Steel, 2006). Although the coeval up-dip part of the underlying deep-water sequences is now absent through later uplift and erosion, their highstand deltas could have backstepped to inner shelf positions, leaving temporary conditions of mudstone-dominated shelf margins (see Poyatos-Moré *et al.*, 2016). This contrasts with the overlying highstand deltas during the Waterford Formation times, which repeatedly reached shelf-edge positions, but accreted most of the sand fraction on the shelf, suggesting that a significant change occurred in the Karoo Basin margin style over time.

From erosion- to accretion-dominated margin style

The change in basin margin style, from erosion- to accretion-dominated, was fundamental in controlling where sand was partitioned over time within the Laingsburg depocentre. Figure 12A is a schematic representation of our understanding of the changing Karoo Basin margin configuration. The time-equivalent up-dip configuration is unknown during the deep-water phase, due to later uplift and erosional removal of the time equivalent shelf and continental stratigraphy. However, we interpret that the early margin had a relatively fixed position and entry point of sediment, perhaps controlled by the underlying basement block configuration (Tankard *et al.*, 2009) and resembled the bypass-dominated fixed margin model of Hadler-Jacobsen *et al.* (2005). Results of this and previous work suggest that this configuration evolved to a more linear sourced, progradational margin style over time (Fig. 12A, see also Jones *et al.*, 2015 and Poyatos-Moré *et al.*, 2016).

A similar change in the nature of the basin margin, from erosion/bypass-dominated to accretion-dominated, was also suggested by Wild *et al.* (2009) for the equivalent slope to shelf succession in the adjacent Tanqua depocentre, and by Ryan *et al.* (2009), in the Porcupine Basin, offshore Ireland. In both cases, during the late progradational margin style, or accretion-dominated phase of the basin-fill, a subsiding shelf was able to accommodate all the sand, which suggests sediment supply broadly kept pace with accommodation generation. However, in the Laingsburg depocentre, increased subsidence in the shelf area and relatively constant sediment supply cannot account for the change from an erosion- to accretion-dominated margin, as under these conditions the basin margin should have remained underfilled. Accretion needed to be enhanced by progressive shallowing of the clinoform slope (both in gradient and depth), which reduced the amount of incision on the slope and sediment bypass to the basin-floor (Fongngern *et al.*, 2016). This is consistent with the overall upward reduction in clinothem thickness in the upper Waterford Formation, and the absence of major conduits on the coeval slope (Poyatos-More *et al.*, 2016) (Figs. 10, 12A).

Regional correlations show the Laingsburg depocentre displays a highly asymmetric sedimentary fill (Fig. 10), indicating a differential subsidence pattern (greater in the W-SW, less in the E-NE), particularly in the deep-water stratigraphy (van der Merwe *et al.*, 2014; Brooks *et al.*, 2018b). These areas of greater subsidence were infilled by progressively lower gradient clinothems as sedimentation outpaced subsidence. The differential subsidence in the early basin fill may have been related to the configuration of pre-existing basement fault blocks (Tankard *et al.*, 2012). However, the subsidence responsible for the increased accumulation of sand on the shelf during the later accretion-dominated phase could also be related to initiation of flexural loading, as the Karoo Basin transitioned into its well documented retro-arc foreland basin setting (De Wit and Ransome, 1992; Veevers *et al*., 1994; López-Gamundí and Rossello, 1998).

Comparison with other basin margin studies

The shelf-edge rollover trajectory and clinoform architecture of the Laingsburg basin margin (Figs. 10, 12A) shows a progressive upward decrease in clinoform slope and length, and an associated change from strongly progradational to aggradational style. This pattern has been also described in the Porcupine Basin, offshore Ireland (Ryan *et al.*, 2009), the mid-Norwegian continental shelf (Bullimore *et al.*, 2005), and the Magallanes Basin margin, Chile (Hubbard *et al.*, 2010; Daniels *et al.*, 2017). The Miocene clinothems of the New Jersey margin (Mountain *et al.*, 2010; Miller, *et al.*, 2013; Proust *et al.*, 2018) also display similar trajectory and gradient evolution, including flat progradational (like Unit G to WfC2), rising aggradational (like WfC 3-5), and flat-to-falling progradational trajectory (like WfC 6-8) (Fig. 12A). However, in the New Jersey example, the dominant process regime had a stronger control than clinoform rollover trajectory on the character and quality of sand onto the foreset and bottomsets segments (Cosgrove *et al.*, 2018). A similar architecture to the Laingsburg depocentre, with an upward-shallowing clinoform geometry and the progressive reduction of sand-rich deep-water systems over time, is observed in cases like the Po River wedge in the Adriatic Sea (Pellegrini *et al.*, 2018), the southern margin of the Neuquén Basin (Loss *et al.*, 2018), and in the Pannonian Basin fill (Leever *et al.*, 2011; Matenco & Andriessen, 2013) (Fig. 12). However, in these cases, the resulting clinoform is due to progradation against confining basin topography, a condition not observed in the present study (Fig. 12).

Results of this work complement studies that have identified a close relationship between shelf-edge trajectory, basin margin-scale stacking patterns and deep-water sedimentation styles (*e.g.* Gong *et al.*, 2015). We propose that differential subsidence and asymmetric basin physiography can influence sediment pathways and styles of deep-water sedimentation through time, and potentially limit the extent, height and gradient of basin margin clinothems, resulting in an overall upward decrease in deep-water sediment delivery and increased accumulation of sand on the shelf during an erosion-to-accretion transition. This study therefore emphasizes the potential influence of inherited basement configuration and changing nature of basin margins through time on clinothem geometry and resulting sediment distribution.

Conclusions

Unit G in the Laingsburg depocentre is a rare example of an exhumed seismic-scale basin margin clinothem, preserving a >60 km long, complete shelf-slope-basin floor transition. A thin, sand-rich, bypass-dominated and wave-influenced topset (shelf) segment is preserved in the south, passing down-dip through the shelf edge rollover zone (SERZ) into a coeval thick and heterolithic foreset (slope), which progressively thins and decreases in grain size into a sand-starved bottomset (basin floor). Along strike, the foreset segment is steeper, dominated by erosive processes and sediment bypass, and displays a marked stepped geometry, with a shallower zone of intraslope sand deposition, and a preserved base-of-slope zone (BOSZ) with sand-rich bottomset deposits.

Unit G is interpreted as part of a composite sequence that records a transition in the large-scale stratigraphic arrangement, from sandstone-rich lowstand systems tract-dominated deep-water sequences, to thicker, highstand systems tract-dominated shallow-marine sequences. This change is related to the transition from an incisional shelf and slope to a younger, accretion-dominated shelf, marking a major change in basin margin style through time. The inherited basin configuration and physiographic evolution of the Karoo Basin margin fundamentally affected the bypass or storage of sediment, and the distribution of seabed topography influenced significantly the along-strike variability of systems tracts and the resulting clinothem geometry. This work demonstrates that mechanisms of sediment transfer and the nature of depositional systems and sedimentary transition zones change through time and space during basin margin evolution. Delivery of coarse clastic material to deep marine settings is not only controlled by relative sea-level changes at or around the shelf-edge rollover zone, but can also be driven by longer-term changes in basin margin physiography and slope angle. This cautions against the use of analogue data from persistently progradational successions that do not account for the influence of inherited basement configuration and changing nature of basin margins through time on clinothem geometry and resulting sediment distribution, with potential implications in predictive basin evolution models.

Acknowledgements

The authors thank the local farmers of the Laingsburg area for permission to undertake field studies on their land, and De Ville Wickens for his help with regional context and logistical support. This work was carried out as part of the SLOPE Phase 4 consortium research project, sponsored by Anadarko, BHP Billiton, BP, ConocoPhillips, ENGIE, Maersk Oil, Murphy, Nexen, Petrobras, Premier Oil, Shell, Statoil, Total, VNG Norge, and Woodside. This manuscript has benefited from the insightful comments and reviews of George Hiley, Migdalys Salazar, Cornel Olariu and Josh Dixon.

References

Ainsworth, R.B., Vakarelov, B.K. & Nanson, R.A. (2011) Dynamic Spatial and Temporal Prediction of Changes in Depositional Processes on Clastic Shorelines: Toward Improved Subsurface Uncertainty Reduction and Management. *American Association of Petroleum Geologists, Bulletin*, **95,** 267-297.

Andersson, P.O.D., Worden, R.H., Hodgson, D.M. & Flint, S. (2004) Provenance Evolution and Chemostratigraphy of a Palaeozoic Submarine Fan-Complex: Tanqua Karoo Basin, South Africa. *Marine and Petroleum Geology*, **21,** 555-577.

Anell, I., Midtkandal, I. & Braathen, A. (2014) Trajectory Analysis and Inferences on Geometric Relationships of an Early Triassic Prograding Clinoform Succession on the Northern Barents Shelf. *Marine and Petroleum Geology*, **54,** 167-179.

Bhattacharya, J.P. & MacEachern, J.A. (2009) Hyperpycnal Rivers and Prodeltaic Shelves in the Cretaceous Seaway of North America. *Journal of Sedimentary Research*, **79,** 184-209.

Brooks, H.L., Hodgson, D.M., Brunt, R.L., Peakall, J., Hofstra, M. & Flint, S.S. (2018a) Deep-Water Channel-Lobe Transition Zone Dynamics: Processes and Depositional Architecture, an Example from the Karoo Basin, South Africa. *Geological Society of America Bulletin*, **130**, 1723-1746

Brooks, H.L., Hodgson, D.M., Brunt, R.L., Peakall, J., Poyatos-Moré, M. & Flint, S.S. (2018b) Disconnected Submarine Lobes as a Record of Stepped Slope Evolution over Multiple Sea-Level Cycles. *Geosphere*, **14,** 1753-1779.

Brunt, R.L., Di Celma, C., Hodgson, D.M., Flint, S.S., Kavanagh, J.P. & van der Merwe, W.C. (2013a) Driving a Channel through a Levee When the Levee Is High: An Outcrop Example of Submarine Down-Dip Entrenchment. *Marine and Petroleum Geology*, **41,** 134-145.

Brunt, R.L., Hodgson, D.M., Flint, S.S., Pringle, J.K., Di Celma, C., Prélat, A. & Grecula, M. (2013b) Confined to Unconfined: Anatomy of a Base of Slope Succession, Karoo Basin, South Africa. *Marine and Petroleum Geology*, **41,** 206-221.

Bullimore, S., Henriksen, S., Liestøl, F.M. & Helland-Hansen, W. (2005) Clinoform Stacking Patterns, Shelf-Edge Trajectories and Facies Associations in Tertiary Coastal Deltas, Offshore Norway: Implications for the Prediction of Lithology in Prograding Systems. *Norwegian Journal of Geology*, **85,** 169-187.

Burgess, P.M. & Prince, G.D. (2015) Non-Unique Stratal Geometries: Implications for Sequence Stratigraphic Interpretations. *Basin Research*, **27,** 351-365.

Carvajal, C. & Steel, R. (2009) Shelf-Edge Architecture and Bypass of Sand to Deep Water: Influence of Shelf-Edge Processes, Sea Level, and Sediment Supply. *Journal of Sedimentary Research*, **79,** 652-672.

Carvajal, C., Steel, R. & Petter, A. (2009) Sediment Supply: The Main Driver of Shelf-Margin Growth. *Earth-Science Reviews*, **96,** 221-248.

Cobain, S.L., Peakall, J. & Hodgson, D.M. (2015) Indicators of Propagation Direction and Relative Depth in Clastic Injectites: Implications for Laminar Versus Turbulent Flow Processes. *Geological Society of America Bulletin*, **127**, 1816-1830.

Cobain, S.L., Hodgson, D.M., Peakall, J. & Shiers, M.N. (2017) An Integrated Model of Clastic Injectites and Basin Floor Lobe Complexes: Implications for Stratigraphic Trap Plays. *Basin Research*, **29,** 816-835.

Cosgrove, G.I., Hodgson, D.M., Poyatos-Moré, M., Mountney, N.P. & McCaffrey, W.D. (2018) Filter or Conveyor? Establishing Relationships between Clinoform Rollover Trajectory, Sedimentary Process Regime, and Grain Character within Intrashelf Clinothems, Offshore New Jersey, USA. *Journal of Sedimentary Research*, **88,** 917-941.

Daniels, B.G., Auchter, N.C., Hubbard, S.M., Romans, B.W., Matthews, W.A. & Stright, L. (2018) Timing of Deep-Water Slope Evolution Constrained by Large-N Detrital and Volcanic Ash Zircon Geochronology, Cretaceous Magallanes Basin, Chile. *GSA Bulletin*, **130,** 438-454.

De Wit, M. & Ransome., I.D.G. (1992) Regional Inversion Tectonics Along the Southern Margin of Gondwana. In: *Inversion Tectonics of the Cape Fold Belt. Karoo and Cretaceous Basins of South Africa.* (Ed. by M. J. De Wit & I. D. G. Ransome), 15-21. A.A. Balkema, Rotterdam.

Deptuck, M.E., Sylvester, Z. & O'Byrne, C. (2012) Pleistocene Seascape Evolution above a "Simple" Stepped Slope Profile- Western Niger Delta. In: *Application of the Principles of Seismic Geomorphology to Continental-Slope and Base-of-Slope Systems: Case Studies from Seafloor and near-Seafloor Analogues. Sepm Society for Sedimentary Geology Special Publication, 99* (Ed. by B. E. Prather, M. E. Deptuck, D. Mohrig, B. Van Hoorn & R. B. Wynn), 199-222.

Dixon, J.F., Steel, R.J. & Olariu, C. (2012a) River-Dominated, Shelf-Edge Deltas: Delivery of Sand across the Shelf Break in the Absence of Slope Incision. *Sedimentology*, **59,** 1133-1157.

Dixon, J.F., Steel, R.J. & Olariu, C. (2012b) Shelf-Edge Delta Regime as a Predictor of Deep-Water Deposition. *Journal of Sedimentary Research*, **82,** 681-687.

Figueiredo, J.J.P., Hodgson, D.M., Flint, S.S. & Kavanagh, J.P. (2010) Depositional Environments and Sequence Stratigraphy of an Exhumed Permian Mudstone-Dominated Submarine Slope Succession, Karoo Basin, South Africa. *Journal of Sedimentary Research*, **80,** 97-118.

Flint, S.S., Hodgson, D.M., Sprague, A.R., Brunt, R.L., Van der Merwe, W.C., Figueiredo, J., Prélat, A., Box, D., Di Celma, C. & Kavanagh, J.P. (2011) Depositional Architecture and Sequence Stratigraphy of the Karoo Basin Floor to Shelf Edge Succession, Laingsburg Depocentre, South Africa. *Marine and Petroleum Geology*, **28,** 658-674.

Fongngern, R., Olariu, C., Steel, R.J. & Krézsek, C. (2016) Clinoform Growth in a Miocene, Para-Tethyan Deep Lake Basin: Thin Topsets, Irregular Foresets and Thick Bottomsets. *Basin Research*, **28,** 770-795.

Fongngern, R., Olariu, C., Steel, R., Mohrig, D., Krézsek, C. & Hess, T. (2018) Subsurface and Outcrop Characteristics of Fluvial-Dominated Deep-Lacustrine Clinoforms. *Sedimentology*, **65,** 1447-1481.

Gomis-Cartesio, L.E., Poyatos-Moré, M., Flint, S.S., Hodgson, D.M., Brunt, R.L. & Wickens, H.D. (2016) Anatomy of a Mixed-Influence Shelf Edge Delta, Karoo Basin, South Africa. In: *Sedimentology of Paralic Reservoirs: Recent Advances* (Ed. by G. J. Hampson, A. D. Reynolds, B. Kostic & M. R. Wells), Geological Society, London, Special Publications, Vol. 444, SP444-5.

Gomis-Cartesio, L.E., Poyatos-Moré, M., Hodgson, D.M. & Flint, S.S. (2018) Shelf-Margin Clinothem Progradation, Degradation and Readjustment: Tanqua Depocentre, Karoo Basin (South Africa). *Sedimentology*, **65,** 809-841.

Gong, C., Wang, Y., Pyles, D.R., Steel, R.J., Xu, S., Xu, Q. & Li, D. (2015) Shelf-Edge Trajectories and Stratal Stacking Patterns: Their Sequence-Stratigraphic Significance and Relation to Styles of Deep-Water Sedimentation and Amount of Deep-Water Sandstoneshelf-Edge Trajectories. *AAPG Bulletin*, **99,** 1211-1243.

Grecula, M., Flint, S., Potts, G., Wickens, D. & Johnson, S. (2003) Partial Ponding of Turbidite Systems in a Basin with Subtle Growth-Fold Topography: Laingsburg-Karoo, South Africa. *Journal of Sedimentary Research* **73,** 603-620.

Grundvåg, S.A., Helland-Hansen, W., Johannessen, E.P., Olsen, A.H. & Stene, S.A. (2014) The Depositional Architecture and Facies Variability of Shelf Deltas in the Eocene Battfjellet Formation, Nathorst Land, Spitsbergen. *Sedimentology*, **61,** 2172-2204.

Gulliford, A.R., Flint, S.S. & Hodgson, D.M. (2014) Testing Applicability of Models of Distributive Fluvial Systems or Trunk Rivers in Ephemeral Systems: Reconstructing 3-D Fluvial Architecture in the Beaufort Group, South Africa. *Journal of Sedimentary Research*, **84,** 1147-1169.

Hadler-Jacobsen, F., Johannessen, E.P., Ashton, N., Henriksen, S., Johnson, S.D. & Kristensen, J.B. (2005) Submarine Fan Morphology and Lithology Distribution: A Predictable Function of Sediment Delivery, Gross Shelf-to-Basin Relief, Slope Gradient and Basin Relief/Topography. In: *Petroleum Geology: North West Europe and Global Perspectives, Proceedings of the 6th Petroleum Geology Conference, London (Uk)* (Ed. by A. G. Doré & B. A. Vining), 1121-1145.

Helland-Hansen, W. & Hampson, G.J. (2009) Trajectory Analysis: Concepts and Applications. *Basin Research*, **21,** 454-483.

Henriksen, S., Hampson, G.J., Helland-Hansen, W., Johannessen, E.P. & Steel, R.J. (2009) Shelf Edge and Shoreline Trajectories, a Dynamic Approach to Stratigraphic Analysis. *Basin Research*, **21,** 445-453.

Hodgson, D.M., Kane, I.A., Flint, S.S., Brunt, R.L. & Ortiz-Karpf, A. (2016) Time-Transgressive Confinement on the Slope and the Progradation of Basin-Floor Fans: Implications for the Sequence Stratigraphy of Deep-Water Deposits. *Journal of Sedimentary Research*, **86,** 73-86.

Hodgson, D.M., Browning, J.V., Miller, K.G., Hesselbo, S., Poyatos-Moré, M., Mountain, G.S. and Proust, J.-N. (2017) Sedimentology, stratigraphic context, and implications of Miocene intrashelf bottomset deposits, offshore New Jersey. *Geosphere*, **14**, 95-114.

Hubbard, S.M., Fildani, A., Romans, B.W., Covault, J.A. & McHargue, T.R. (2010) High-Relief Slope Clinoform Development: Insights from Outcrop, Magallanes Basin, Chile. *Journal of Sedimentary Research*, **80,** 357-375.

Johnson, M.R., van Vuuren, C.J., Visser, J.N.J., Cole, D.I., Wickens, H.d.V., Christie, A.D.M., Roberts, D.L. & Brandl, G. (2006) Sedimentary Rocks of the Karoo Supergroup. In: *The Geology of South Africa* (Ed. by M. R. Johnson, C. R. Anhaeusser & R. J. Thomas), 461-499, Geological Society of South Africa and Council for Geoscience, Pretoria.

Jones, G.E.D., Hodgson, D.M. & Flint, S.S. (2013) Contrast in the Process Response of Stacked Clinothems to the Shelf-Slope Rollover. *Geosphere*, **9,** 299-316.

Jones, G.E.D., Hodgson, D.M. & Flint, S.S. (2015) Lateral Variability in Clinoform Trajectory, Process Regime, and Sediment Dispersal Patterns Beyond the Shelf-Edge Rollover in Exhumed Basin Margin-Scale Clinothems. *Basin Research*, **27,** 657-680.

Koo, W.M., Olariu, C., Steel, R.J., Olariu, M.I., Carvajal, C.R. & Kim, W. (2016) Coupling between Shelf-Edge Architecture and Submarine-Fan Growth Style in a Supply-Dominated Margin. *Journal of Sedimentary Research*, **86,** 613-628.

Laugier, F.J. & Plink-Björklund, P. (2016) Defining the Shelf Edge and the Three-Dimensional Shelf Edge to Slope Facies Variability in Shelf-Edge Deltas. *Sedimentology*, **63,** 1280-1320.

LEEVER, K.A., MATENCO, L., GARCIA-CASTELLANOS, D. & CLOETINGH, S.A.P.L. (2011) The Evolution of the Danube Gateway between Central and Eastern Paratethys (Se Europe): Insight from Numerical Modelling of the Causes and Effects of Connectivity between Basins and Its Expression in the Sedimentary Record. *Tectonophysics*, **502,** 175-195.

LINOL, B., CHERE, N., MUEDI, T., NENGOVHELA, V. & DE WIT, M.J. (2016) Deep Borehole Lithostratigraphy and Basin Structure of the Southern Karoo Basin Re-Visited. In: *Origin and Evolution of the Cape Mountains and Karoo Basin* (Ed. by B. Linol & M. J. de Wit), 3-16. Springer International Publishing, Cham.

LÓPEZ-GAMUNDÍ, O.R. & ROSSELLO, E.A. (1998) Basin Fill Evolution and Paleotectonic Patterns Along the Samfrau Geosyncline: The Sauce Grande Basin–Ventana Foldbelt (Argentina) and Karoo Basin–Cape Foldbelt (South Africa) Revisited. *Geologische Rundschau*, **86,** 819-834.

LOSS, M.L., BRINKWORTH, W., VOCATURO, G., OLARIU, C. & STEEL, R. (2018) Morphology and Evolution of Basin-Margin Clinoform Growth, Cuyo Group, Neuquen Basin; Seismic Examples Enhanced by Outcrop Observations. *EGU General Assembly 2018, 8–13 April, Vienna, Austria*, Geophysical Research Abstracts. **20**.

MADOF, A.S., HARRIS, A.D. & CONNELL, S.D. (2016) Nearshore Along-Strike Variability: Is the Concept of the Systems Tract Unhinged? *Geology*, **44,** 315-318.

MARTINSEN, O.J. & HELLAND-HANSEN, W. (1995) Strike Variability of Clastic Depositional Systems: Does It Matter for Sequence-Stratigraphic Analysis? *Geology*, **23,** 439-442.

MATENCO, L. & ANDRIESSEN, P. (2013) Quantifying the Mass Transfer from Mountain Ranges to Deposition in Sedimentary Basins: Source to Sink Studies in the Danube Basin–Black Sea System. *Global and Planetary Change*, **103,** 1-18.

MILLER, K.G., MOUNTAIN, G.S., BROWNING, J.V., KATZ, M.E., MONTEVERDE, D., SUGARMAN, P.J., ANDO, H., BASSETTI, M.A., BJERRUM, C.J., HODGSON, D., HESSELBO, S., KARAKAYA, S., PROUST, J.-N. & RABINEAU, M. (2013) Testing Sequence Stratigraphic Models by Drilling Miocene Foresets on the New Jersey Shallow Shelf. *Geosphere*, **9,** 1236-1256.

MORRIS, E.A., HODGSON, D.M., BRUNT, R.L. & FLINT, S.S. (2014) Origin, Evolution and Anatomy of Silt-Prone Submarine External Levées. *Sedimentology*, **61,** 1734-1763.

MOUNTAIN, G.S., PROUST, J.-N., MCINROY, D. & COTTERILL, C. (2010) Proceedings of the Integrated Ocean Drilling Program, Volume 313: Tokyo, Integrated Ocean Drilling Program Management International, Inc.

MULDER, T., SYVITSKI, J.P.M., MIGEON, S., FAUGÈRES, J.C. & SAVOYE B. (2003) Hyperpycnal Turbidity Currents: Initiation, Behavior and Related Deposits: A Review. *Marine and Petroleum Geology 20***,** 861-882.

MUTTI, E. & NORMARK, W.R. (1987) Comparing Examples of Modern and Ancient Turbidite Systems: Problems and Concepts. In: *Marine Clastic Sedimentology: Concept and Case Studies* (Ed. by J. K. Leggett & G. G. Zuffa), 1-38. Graham & Trotman, London.

MUTTI, E. & NORMARK, W.R. (1991) An Integrated Approach to the Study of Turbidite Systems. In: *Seismic Facies and Sedimentary Processes of Submarine Fans and Turbidite Systems* (Ed. by P. Weimer & H. Link), 75-107. Springer-Verlag, New York.

OLARIU, C. & STEEL, R.J. (2009) Influence of Point-Source Sediment-Supply on Modern Shelf-Slope Morphology: Implications for Interpretation of Ancient Shelf Margins. *Basin Research*, **21,** 484-501.

Olariu, M.I., Carvajal, C.R., Olariu, C. & Steel, R.J. (2012) Deltaic Process and Architectural Evolution During Cross-Shelf Transits, Maastrichtian Fox Hills Formation, Washakie Basin, Wyoming. *American Association of Petroleum Geologists, Bulletin*, **96,** 1931-1956.

Pángaro, F., Ramos, V.A. & Pazos, P.J. (2016) The Hesperides Basin: A Continental-Scale Upper Palaeozoic to Triassic Basin in Southern Gondwana. *Basin Research*, **28,** 685-711.

Patruno, S., Hampson, G.J. & Jackson, C.A.L. (2015) Quantitative Characterisation of Deltaic and Subaqueous Clinoforms. *Earth-Science Reviews*, **142,** 79-119.

Pellegrini, C., Asioli, A., Bohacs, K.M., Drexler, T.M., Feldman, H.R., Sweet, M.L., Maselli, V., Rovere, M., Gamberi, F. & Dalla Valle, G. (2018) The Late Pleistocene Po River Lowstand Wedge in the Adriatic Sea: Controls on Architecture Variability and Sediment Partitioning. *Marine and Petroleum Geology*, **96,** 16-50.

Plink-Björklund, P. & Steel, R.J. (2004) Initiation of Turbidity Currents: Outcrop Evidence for Eocene Hyperpycnal Flow Turbidites. *Sedimentary Geology*, **165,** 29-52.

Porębski, S.J. & Steel, R.J. (2003) Shelf-Margin Deltas: Their Stratigraphic Significance and Relation to Deepwater Sands. *Earth-Science Reviews*, **62,** 283-326.

Porębski, S.J. & Steel, R.J. (2006) Deltas and Sea-Level Change. *Journal of Sedimentary Research*, **76,** 390-403.

Poyatos-Moré, M., Jones, G.D., Brunt, R.L., Hodgson, D.M., Wild, R.J. & Flint, S.S. (2016) Mud-Dominated Basin-Margin Progradation: Processes and Implications. *Journal of Sedimentary Research*, **86,** 863-878.

Prather, B.E., Booth, J.R., Steffens, G.S. & Craig, P.A. (1998) Classification, Lithologic Calibration, and Stratigraphic Succession of Seismic Facies of Intraslope Basins, Deep-Water Gulf of Mexico. *AAPG Bulletin*, **82,** 701-728.

Prather, B.E., O'Byrne, C., Pirmez, C. & Sylvester, Z. (2017) Sediment Partitioning, Continental Slopes and Base-of-Slope Systems. *Basin Research*, **29,** 394-416.

Prélat, A. & Hodgson, D.M. (2013) The Full Range of Turbidite Bed Thickness Patterns in Submarine Lobes: Controls and Implications. *Journal of the Geological Society*, **170,** 209-214.

Prélat, A., Pankhania Shyam, S., Jackson, C., A-L. & Hodgson, D.M. (2015) Slope Gradient and Lithology as Controls on the Initiation of Submarine Slope Gullies; Insights from the North Carnarvon Basin, Offshore Nw Australia. *Sedimentary Geology*, **329**, 12-17.

Proust, J.-N., Pouderoux, H., Ando, H., Hesselbo, S.P., Hodgson, D.M., Lofi, J., Rabineau, M. & Sugarman, P.J. (2018) Facies Architecture of Miocene Subaqueous Clinothems of the New Jersey Passive Margin: Results from Iodp-Icdp Expedition 313. *Geosphere*, **14,** 1564-1591.

Pyles, D.R. & Slatt, R.M. (2007) Applications to Understanding Shelf Edge to Base-of-Slope Changes in Stratigraphic Architecture of Prograding Basin Margins: Stratigraphy of the Lewis Shale, Wyoming, USA. In: *Atlas of Deepwater Outcrops: Aapg Studies in Geology 56* (Ed. by T. H. Nilsen, R. D. Shew, G. S. Steffens & J. R. J. Studlick), 485-489.

Pysklywec, R.N. & Mitrovica, J.X. (1999) The Role of Subduction-Induced Subsidence in the Evolution of the Karoo Basin. *Journal of Geology*, **107,** 155-164.

Rubidge, B.S., Hancox, P.J. & Catuneanu, O. (2000) Sequence Analysis of the Ecca-Beaufort Contact in the Southern Karoo of South Africa. *South African Journal of Geology*, **1,** 81-96.

RYAN, M.C., HELLAND-HANSEN, W., JOHANNESSEN, E.P. & STEEL, R.J. (2009) Erosional Vs. Accretionary Shelf Margins: The Influence of Margin Type on Deepwater Sedimentation: An Example from the Porcupine Basin, Offshore Western Ireland. *Basin Research*, **21,** 676-703.

SANCHEZ, C.M., FULTHORPE, C.S. & STEEL, R.J. (2012) Miocene Shelf-Edge Deltas and Their Impact on Deepwater Slope Progradation and Morphology, Northwest Shelf of Australia. *Basin Research*, **24,** 683-698.

SCHEFFLER, K., BUEHMANN, D. & SCHWARK, L. (2006) Analysis of Late Palaeozoic Glacial to Postglacial Sedimentary Successions in South Africa by Geochemical Proxies – Response to Climate Evolution and Sedimentary Environment. *Palaeogeography, Palaeoclimatology, Palaeoecology*, **240,** 184-203.

SINCLAIR, H. & TOMASSO, M. (2002) Depositional Evolution of Intra-Slope Turbidite Sub-Basins. *Journal of Sedimentary Research*, **72,** 452-457.

SIXSMITH, P.J., FLINT, S.S., WICKENS, H.D.V. & JOHNSON, S.D. (2004) Anatomy and Stratigraphic Development of a Basin Floor Turbidite System in the Laingsburg Formation, Main Karoo Basin, South Africa. *Journal of Sedimentary Research*, **74,** 239-254.

SMITH, R. (2004a) Turbidite Systems Influenced by Structurally Induced Topography in the Multi-Sourced Welsh Basin. In: *Confined Turbidite Systems. Geological Society, London, Special Publications. V. 222* (Ed. by S. A. Lomas & P. Joseph), 209-228.

SMITH, R. (2004b) Silled Sub-Basins to Connected Tortuous Corridors: Sediment Distribution Systems on Topographically Complex Sub-Aqueous Slopes. In: *Confined Turbidite Systems. Geological Society, London, Special Publications. V. 222* (Ed. by S. A. Lomas & P. Joseph), 23-43.

SPYCHALA, Y.T., HODGSON, D.M., FLINT, S.S. & MOUNTNEY, N.P. (2015) Constraining the Sedimentology and Stratigraphy of Submarine Intraslope Lobe Deposits Using Exhumed Examples from the Karoo Basin, South Africa. *Sedimentary Geology*, **322,** 67-81.

STEEL, R. & OLSEN, T. (2002). *Clinoforms, Clinoform Trajectories and Deepwater Sands.* Gulf Coast Section SEPM Foundation, 22nd Annual Research Conference Special Publication, SEPM, CD-ROM.

STEEL, R.J., POREBSKI, S.J., PLINK-BJORKLUND, P., MELLERE, D. & SCHELLPEPER, M. (2003) Shelf-Edge Delta Types and Their Sequence-Stratigraphic Relationships. *Shelf Margin Deltas and Linked Down Slope Petroleum Systems: Global Significance and Future Exploration Potential*. Houston, Texas. December 7-10.**,** 205-230.

STEVENSON, C.J., JACKSON, C.A.-L., HODGSON, D.M., HUBBARD, S.M. & EGGENHUISEN, J.T. (2015) Deep-Water Sediment Bypass. *Journal of Sedimentary Research*, **85,** 1058-1081.

TANKARD, A., WELSINK, H., AUKES, P., NEWTON, R. & STETTLER, E. (2009) Tectonic Evolution of the Cape and Karoo Basins of South Africa. *Marine and Petroleum Geology*, **26,** 1379-1412.

TANKARD, A., WELSINK, H., AUKES, P., NEWTON, R. & STETTLER, E. (2012) Chapter 23: Geodynamic Interpretation of the Cape and Karoo Basins, South Africa. In: *Phanerozoic Passive Margins, Cratonic Basins and Global Tectonic Maps* (Ed. by D. G. Rioberts & A. W. Bally), 869-945. Elsevier, Amsterdam.

VAN DER MERWE, W.C., HODGSON, D.M. & FLINT, S.S. (2009) Widespread Syn-Sedimentary Deformation on a Muddy Deep-Water Basin-Floor: The Vischkuil Formation (Permian), Karoo Basin, South Africa. *Basin Research*, **21,** 389-406.

van der Merwe, W.C., Flint, S.S. & Hodgson, D.M. (2010) Sequence Stratigraphy of an Argillaceous, Deepwater Basin-Plain Succession: Vischkuil Formation (Permian), Karoo Basin, South Africa. *Marine and Petroleum Geology*, **27,** 321-333.

van der Merwe, W.C., Hodgson, D.M. & Flint, S.S. (2011) Origin and Terminal Architecture of a Submarine Slide: A Case Study from the Permian Vischkuil Formation, Karoo Basin, South Africa. *Sedimentology*, **58,** 2012-2038.

van der Merwe, W.C., Hodgson, D.M., Brunt, R.L. & Flint, S.S. (2014) Depositional Architecture of Sand-Attached and Sand-Detached Channel-Lobe Transition Zones on an Exhumed Stepped Slope Mapped over a 2500 Km2 Area. *Geosphere*, **10,** 1076-1093.

Van Lente, B. (2004) Chemostratigraphic Trends and Provenance of the Permian Tanqua and Laingsburg Depocentres, South Western Karoo Basin, South Africa. Unpublished Ph.D. Thesis, University of Stellenbosch, South Africa.

Veevers, J.J., Cole, D.I. & Cowan, E.J. (1994) Southern Africa: Karoo Basin and Cape Fold Belt. In: *Permian-Triassic Pangean Basins and Foldbelts Along the Panthalassan Margin of Gondwanaland: Geological Society America, Memoir 184* (Ed. by J. J. Veevers & C. M. Powell), 223-279.

Viljoen, J. (1994) Sedimentology of the Collingham Formation, Karoo Supergroup. *South African Journal of Geology*, **97,** 167-183.

Vorster, C. (2013) Laser Ablation Icp-Ms Age Determination of Detrital Zircon Populations in the Phanerozoic Cape and Lower Karoo Supergroups (South Africa) and Correlatives in Argentina. Phd Thesis, University of Johannesburg, South Africa.

Wild, R., Flint, S.S. & Hodgson, D.M. (2009) Stratigraphic Evolution of the Upper Slope and Shelf Edge in the Karoo Basin, South Africa. *Basin Research*, **21,** 502-527.

Wilson, A., Flint, S., Payenberg, T., Tohver, E. & Lanci, L. (2014) Architectural Styles and Sedimentology of the Fluvial Lower Beaufort Group, Karoo Basin, South Africa. *Journal of Sedimentary Research*, **84,** 326-348.

Winker, C. & Booth, J.R. (2000) Sedimentary Dynamics of the Salt-Dominated Continental Slope, Gulf of Mexico: Integration of Observations from the Seafloor, near-Surface, and Deep Subsurface. *Deep-Water Reservoirs of the World: Proc. GCSSEPM 20th Annu. Res. Conf***,** 1059-2086.

Wynn, R.B., Kenyon, N.H., Masson, D.G., Stow, D.A.V. & Weaver, P.P.E. (2002a) Characterization and Recognition of Deep-Water Channel-Lobe Transition Zones. *AAPG Bulletin*, **86,** 1441-1462.

Wynn, R.B., Piper, D.J.W. & Gee, M.J.R. (2002b) Generation and Migration of Coarse-Grained Sediment Waves in Turbidity Current Channels and Channel–Lobe Transition Zones. *Marine Geology*, **192,** 59-78.

Zavala, C., Arcuri, M., Gamero, H., Contreras, C. & Di Meglio, M. (2011) A Genetic Facies Tract for the Analysis of Sustained Hyperpycnal Flow Deposits. In: *Sediment Transfer from Shelf to Deep Water - Revisiting the Delivery System. Aapg Studies in Geology 61* (Ed. by Eds R.M. Slatt & C. Zavala), 31-51.

Figure captions

Fig. 1. Location map of the study area in the Laingsburg depocentre, showing the outcrop belt of the Fort Brown (dark grey) and Waterford (light grey) formations, and the different stratigraphic sections included in this study.

Fig. 2. Regional stratigraphic correlation of the upper Ecca Group in the northern part of the Laingsburg depocentre, showing the main stratigraphic units, from the basin-floor Collingham Formation, to the top of the WfC8 parasequence in the shelf/deltaic deposits of the Waterford Formation. Note the asymmetric thickness distribution of the deep-water units (Vischkuil Formation to Unit F), and the effect of this on the geometry of the overlying seaward-dipping and wedge-shaped units (Unit G to WfC8), associated with the progradation of basin margin clinothems. SERZ = shelf edge rollover zone, CLTZ = channel-lobe transition zone, SOT = shoreface-offshore transition deposits.

Fig. 3. (A) Palaeocurrent data from Unit G, showing consistency with E to ENE depositional dip direction. (B) Thickness map of the mudstone package between top of Unit G and base of WfC2. (C) Thickness map of Unit G. (D) Thickness map of the mudstone package between top of Unit F and base of Unit G.

Fig. 4. Correlation fence-diagram of Unit G in the Laingsburg depocentre, reconstructed from selected logs, showing the along-strike stratigraphic architecture and facies variability of Unit G, from south to north. See the position of different panels in Figure 1. See Table 2 for further information about facies associations.

Fig. 5. Detail of BS2 type locality showing facies associations and depositional features found in topset (shelf) settings of Unit G. (A) BS2 log from the Baviaans South panel (see colour code in Fig. 4). (B) Erosive sandstone filled bypass scours (base Unit G). (C) Wave ripples and hummocky

923 cross-stratified sandstones formed above storm wave base. (D) Coarsening-upward lower
924 shoreface deposits (top Unit G).

925 Fig. 6. Detail of facies associations and depositional features found in intermediate upper foreset
926 (slope) type localities of Unit G in the southern (BN2 log) and northern (FB2 log) areas of the
927 Laingsburg depocentre. Unit G in intermediate settings differs significantly across depositional
928 strike. (A) FB2 log from the Baviaans North panel (see colour code in Fig. 4). (B) Sand-filled gulleys
929 with mudstone clast-rich erosive surfaces (FB4 locality). (C) Very fine sandstones/siltstones with
930 sigmoidal bedforms (FB2 locality). (D) Slumped heterolithic sandstone/siltstone deposits (FB1
931 locality). (E) BN2 log from the Zoutkloof/Faberskraal panel. (F) Coarsening to fining up log section
932 of Unit G beyond the SERZ (BS4 locality). (G) Inversely-to-normally graded beds with ripple cross
933 lamination (BS4 locality). (H) Polished hand speciment of bioturbated heterolithic deposits (BS4
934 locality).

935 Fig. 7. Detail of FB6 type locality showing facies associations and depositional features found in
936 the lower foreset (slope) of Unit G in the northern areas of the Laingsburg depocentre. (A) FB6
937 log from the Zoutkloof/Faberskraal panel (see colour code in Fig. 4). (B) UAV photo of Unit G at
938 the FB6 locality, with amalgamated erosive sandstones cutting into slope mudstones. (C) Highly
939 incisional erosive surface at the base of stacked-sandstone unit. (D) Mud-clast conglomerates
940 draping erosion and amalgamation surfaces. (E) Erosive, sharp top surface of sandstone unit
941 filled by thin-bedded heterolithics.

942 Fig. 8. Detail of FB8 type locality showing facies associations and depositional features found in
943 bottomset (basin) settings of Unit G in the northern areas of the Laingsburg depocentre. (A) FB8
944 log from the Zoutkloof/Faberskraal panel (see colour code in Fig. 4). (B) UAV photo of Unit G at
945 the FB8 locality, with erosive lobes cutting into basinal mudstones, with sand injections. (C)
946 Basin-floor lobe structureless sandstone. (D) Stacked hybrid-event beds.

Fig. 9. Conceptual block diagram of Unit G, based on data observations, showing the complex lateral variability between an accretion-dominated, shelf-edge rollover zone preserved in the south, with a coeval thick and sandy foreset passing to a sand-starved bottomset, and a steeper, erosion-dominated and stepped foreset in the north, with sandstone-filled intra-slope topography and passing downslope to sand-rich basin floor fan deposits through a preserved base-of-slope zone.

Fig. 10. A) Seismic-scale correlation panel of the Ecca Group (from Collingham Formation to Waterford Formation) in the Laingsburg depocentre, reconstructed from integrating data from this study with regional correlation panels from previous works (Flint *et al.*, 2011; van der Merwe *et al.*, 2014; Jones *et al.*, 2015). Field correlation horizons were recreated as well top surfaces in PETREL. The succession is datumed on the flooding surface above the WfC8 parasequence (Jones *et al.*, 2015), and shows the spatial-temporal evolution of the basin fill and the position of sedimentary transition zones (SERZ and BOSZ) through time. B) Overlap of top Unit F, top Unit G and top WfC 8 surfaces, showing development of the seaward-dipping, wedge-shaped mudstone packages between Units F and G and between Units G and WfC 1.

Fig. 11. A. Schematic representation of the long-term change from a bypass-dominated margin with well-developed lowstand-dominated deep-water sequences, to an accretion-dominated shelf, characterized by shallow marine deposits and thick highstand systems tract. B. Relative thicknesses of systems tracts between the underlying deep-water sequences, Unit G, and the overlying shallow-marine sequences.

Fig. 12. Comparison of the Karoo Basin margin with other published examples. A. Conceptual diagram showing the evolution of the Karoo Basin margin style through time. Grey box represents window of outcrop exposure. B) Seismic profile and C) line drawing of the late Pleistocene Po River Lowstand Wedge (PRLW) in yellow, showing development of clinothems within a confining basin configuration. D) Conceptual stratigraphic section of the PRLW. From

Pellegrini *et al*. (2018). E) Interpreted seismic profile of the Jurassic Cuyo Group clinothems in the southern margin of the Neuquén Basin (Loss *et al*., 2018). F) Synthetic numerical modelling of the clinoform succession of the Panonian Basin (Leveer *et al*., 2011). Note the similarity with the evolution proposed for the Karoo Basin margin with limited early topset accommodation, continual bottomset aggradation, progressive shallowing and resulting increase in shelf width and decrease in basinward sand delivery.

Table 1. Unit G facies classification, description and interpretation of the main processes and environments of deposition. For further information about facies associations see Table 2.

Table 2. Facies associations of Unit G, with the typical lithofacies found, and a summary of the main characteristics. Same colour code as in Figure 4.

LITHOFACIES	STRUCTURES	BED THICKNESS	BED BOUNDARIES	OUTCROP THICKNESS/GEOMETRY	TRACES AND OTHER	PROCESS INTERPRETATION	FACIES ASSOCIATION
Fa1 Structureless mudstone	Typically structureless. Little to no internal stratification.	1 cm - 1 m.	Normally gradational, occasionally sharp bases. Sharp, occasionally erosional tops.	From 10s cm to 10s m-thick. Gradual thinning down dip. Mappable laterally and down-dip for 10's km.	No bioturbation observed. Concretionary nodules and ash beds.	Hemipelagic suspension fallout and rare dilute turbidity currents.	Basinal mudstone.
Fa2 Structureless to thinly laminated siltstone	Typically structureless, but thin coaser laminations can be observed.	1 cm - 1 m.	Normally gradational, occasionally sharp and rare erosional bases. Sharp, occasionally erosional tops.	From 10s of cm to 10s of m-thick. Gradual thinning down dip. Extensive (10s km).	None.	Settling of fine grained fraction of dilute turbidity currents.	Basinal mudstone, prodelta.
Fa3 Rhythmically bedded siltstone and mudstone	Siltstone beds are structureless with occasional planar laminations.	< 1-10 cm, beds thin and fine upwards.	Gradational bases and tops.	<5-20 m-thick. Difficult to follow for more than 1km at outcrop.	None.	Dilute turbidite flows with periods of shutdown and pelagic sedimentation.	Channel (abandonment).
Fa4 Siltstone-prone interbedded sandstone and siltstone	Very fine sandstones often structureless but also wavy, ripple and parallel laminated. Siltstones planar laminated.	< 5-20 cm. (>50% siltstones)	Gradational bases and tops.	Packages range from 10 m to >100 m-thick. Individual thin-beds traceable for up to 100 m. Packages traceable for up 10s km.	Some areas can be intensely bioturbated. Few erosion surfaces associated with bed dip changes above.	Dilute turbidite flows. Bioturbated intervals from periods between events or changes in oxygen/nutrient.	Channel (margin), prodelta, shoreface-offshore transition (SOT), degraded slope, levee, lobe off-axis, lobe fringe.
Fa5 Sandstone-prone interbedded sandstone and siltstone	Very fine sandstones include wavy, aggradational, planar, current ripple, climbing and stoss-side preserved climbing ripple lamination. Siltstones planar laminated.	2-15 cm. (>50% sandstones)	Gradational bases Occasional sharp, non-erosive. Often gradational tops.	Packages up to 150 m in thickness. Individual thin-beds traceable for up to 250 m. Packages traceable for up to 10s km laterally.	Erosion surfaces and amalgamated contacts observed.	Higher rate of deposition. Aggradational facies, with some erosion surfaces. The higher the sand content, the closer to the feeder system.	Channel (axis, margin), delta front, shoreface, prodelta, shoreface-offshore transition (SOT), degraded slope, levee, channel-lobe transition zone, lobe (off-axis, fringe).
Fa6 Thick-bedded structureless sandstone	Very fine to fine-grained. Normally massive. Occasional dewatering pipes and dishes.	< 10 - 200 cm.	Sharp based, often shows large degree of erosion. Normally sharp tops.	<1 m to amalgamated sections of >30 m-thick. 100 – 400 m in width. 100's m of down-dip extent.	Widespread amalgamation along erosive surfaces.	Medium-to-high density flows escaping confinement and deposited rapidly. High rate of deposition.	Channel (axis), delta front, degraded slope, channel-lobe transition zone, lobe (axis).

Fa7 Structured sandstone	Very fine to fine-grained. Current and climbing ripples common. Cross-beds up to 50 cm-high. Soft-sediment deformation and mudstone drapes. Little mud material.	5-70 cm.	Sharp bases. Gradational tops, commonly rippled.	Range 5 - 200 cm, mostly 5 - 30 cm-thick. Individual beds continuous for >100 m.	Common erosion surfaces associated with multidirectional current ripple laminae. Little bioturbation.	Medium-to-high density flows escaping confinement and deposited rapidly. Evidence of a high rate of deposition.	Channel (axis), degraded slope, channel-lobe transition zone, lobe (axis, off-axis).
Fa8 Normally-graded, moderate to well-sorted sandstone	Very fine to fine-grained. Structureless, parallel bedding, ripple lamination.	5 – 50 cm.	Sharp or gradational, loaded base. Sharp or gradational top, commonly rippled.	Packages are in the range of 2-4 m thick. Individual beds tabular at outcrop scale. Units amalgamate and display sheet or lenticular bodies that extend 10s to 100s of m.	Amalgamation and dewatering common. Mudclast-rich bases.	Deposition from waning medium to low-density flow conditions.	Channel (axis, margin), delta front, prodelta, shoreface-offshore transition, lobe (axis, off-axis).
Fa9 Inverse to normally-graded sandstone	Very fine to fine-grained. Structureless or parallel bedding. Occasional ripple or climbing ripple lamination.	5 – 50 cm.	Sharp or gradational bases and tops.	Packages are in the range of 2-4 m thick. Individual beds tabular at outcrop scale. Units amalgamate and display sheet or lenticular bodies that extend 10s to 100s of m.	Plant debris and mica, and development of composite (waxing-waning) beds.	Waxing to waning flow deposition in river-flood periods.	Delta front, prodelta, shoreface-offshore transition.
Fa10 Parallel-bedded sandstone	Very fine to fine-grained. Upper phase plane bed.	20 cm – >1 m.	Sharp erosive base, usually loaded. Rarely gradational. Sharp erosive top, rarely gradational.	Packages are in the range of 2 - 4 m thick. Individual beds tabular at outcrop scale. Units amalgamate and display sheet or lenticular bodies that extend 10s to 100s of m.	Parting lineation, mud clasts, oxidized organic matter and plant fragments observed in parallel laminae.	Late stage of rapid flow deposition under upper phase plane bed conditions.	Channel (axis), delta front, lobe (axis).
Fa11 Unidirectional ripple-laminated sandstone	Very fine-grained. Unidirectional ripple lamination.	10 - 50 cm.	Sharp erosive base and top.	Packages up to 3 m thick. Individual beds tabular to lenticular at outcrop scale. Units display a sheet to wedge geometry over 10s of m to several 100s m.	None.	Traction features developed under lower flow regime conditions. Asymmetrical current ripples produced by unidirectional flows.	Channel (axis, margin), delta front, prodelta, lobe (axis, off-axis)
Fa12 Wavy or wave ripple-laminated sandstone	Very fine to fine-grained. Micro HCS, symmetrical ripple laminae, low angle cross lamination.	10 - 50 cm.	Bed bases are sharp. Packages have gradational bases. Bed tops are sharp to gradational. Packages generally have gradational tops.	Packages up to 4 m thick. Individual beds tabular to lenticular at outcrop scale. Units display a sheet to wedge geometry over 10s of m to several 100s m.	Well-sorted, rounded grains. Common superimposition of interference ripples.	Alternating periods of rapid deposition and reworking by storm and wave generated oscillatory currents.	Shoreface, shoreface-offshore transition.
Fa13 Combined-flow cross-bedded sandstone	Very fine to fine-grained. Low angle, swaley and hummocky cross-stratification.	20 cm – 1 m+.	Gradational base. Sharp erosive or gradational top.	Packages in the range of 2 - 4 m thick. Locally occurring lenticular geometries with occasional scours; pinching and swelling of beds. Units amalgamate and display tabular sheet bodies that extend 10s to 100s of m.	Amalgamation common. Mud clasts, oxidized organic matter and plant fragments observed in the cross-sets.	Migration of subaqueous bedforms affected by combined flows.	Shoreface.

Fa14 Climbing ripple-laminated sandstone	Very fine-grained. Current and/or low angle climbing ripple lamination.	20 - 50 cm.	Sharp erosive bases and tops.	Packages up to 3 m thick. Individual beds tabular to lenticular at outcrop scale. Units can amalgamate and display delta scale clinothems that thin and separate down dip over 2 km. Lateral extent is narrow (< 6 km).	Locally with stoss and lee side of bedforms preserved. High terrigenous content and lack of wave influence.	Deposited by unidirectional currents under lower flow regime conditions and/or high energy flows exiting confinement.	Channel (axis, margin), delta front, levee, lobe (axis, off-axis)
Fa15 Sigmoidal sandstone	Very fine-grained. Sigmoidal shaped bedforms. Stoss-side preserved climbing ripple lamination.	2-30 cm.	Sharp bases. Gradational tops, unis become finer thinner upwards.	Packages <5-25 m thick. Individual thin beds traceable for +250 m. Packages traceable for up to 10s km laterally.	Aggradational facies, with some small-scale erosion features cutting 2 - 10 cm and <50 cm in width.	Medium-to-high density flows escaping confinement and deposited rapidly. Evidence of a high rate of deposition.	Levee, lobe (axis).
Fa16 Scoured siltstone and sandstone	Very fine sandstones often structureless. Siltstones planar laminated. Soft sediment deformation common.	2 cm - 1.2 m.	Sharp or erosive, uneven bases. Sharp and erosive, irregular tops overlain by bypass lags or thinly laminated siltstone.	Amalgamated packages 3-4 m thick. Occurring in areas up to several kms in width and length.	Bedded siltstone with lenticular and poorly sorted silty sandstones overlying and cut by erosional surfaces. Scours can be asymmetric down dip with steeper headwalls < 3- 15 m in length, 1-3 m in width and < 1 m in depth.	Erosion by numerous by-passing turbidity currents.	Channel-lobe transition zone.
Fa17 Mudclast conglomerate and mudclast mantled surfaces (MCMS)	Tightly packed mudstone clasts draping erosive surfaces. From high concentration clast supported to matrix supported conglomerates.	MCMS one or two clasts thick.	Sharp and erosional bases, normally planar with local topography related to the substrate erodability. Typically overlain by thin bedded bypass facies. Minimal thickness means easily lost to erosion.	Local accumulations in scoured depressions 5 - 10 cm-thick. Can drape the full width of channels (50-400 m), except where incised by later erosion. MCMS can also drape downstream side of channel bars.	Well-rounded clasts, <1-4 cm diameter, up to 20 cm. Clast-rich zone generally preserved at/near the base of sand beds as MCMS and/or mud clast conglomerate. Locally medium sandstone present.	Mudclasts deposited as a channel lag/drape. Clasts can show secondary injection. MCMS and mud clast conglomerate deposited/moved in traction beneath confined flows.	Channel (axis), channel-lobe transition zone, (lobe axis).
Fa18 Injectite	Internally structureless very fine sandstone. Bounding surfaces show hydroplastic structures due to erosion of the dyke/sill walls during the injection process.	< 1 cm - 10s of m.	Very sharp bases and tops.	Sub-centimetre scale to 10s of m-thick. Dykes 2-25 cm wide, with exceptional 100's m-wide. Can penetrate m to 10s of m-deep. Sills cm to m-thick. Can be traceable for 100's of m.	Very clean pale coloured sandstones. Vertical dykes with ptygmatic folding by compaction of host mudstones.	Seismicity and rapid fluid migration by overpressure into parent sands, rapid burial or instability of overlying sediments. Fluidized sand propagates through weaknesses (bedding planes and fractures) of surrounding siltstone.	Channel (axis), lobe (axis), pinch out areas
Fa19 Folded and megaclast deposits	Dewatering structures and syn-sedimentary faults.	cm - 10s of m.	Gradational to sharp bases and tops.	Up to 10's of m-thick. Traceable for up to several km.	Clasts vary in scale from small 10's cm scale. Fractured and disaggregated at edges. Internal bedding is well preserved within clasts.	Folded strata formed as slumps and slides remobilise primary bedding, undergoing ductile deformation. Clast and megaclasts formed as cohesive material is remobilised as slides and undergoing only brittle deformation.	Channel (axis), degraded slope, channel-lobe transition zone.

Fa20 Hybrid event bed (HEB's)	Dewatering structures, rare planar lamination	20 cm - 1.5 m.	Sharp bases, can be erosive. Sharp tops.	Creates 10's m-thick packages. Occurring in outcrop continuously for several kilometres.	Two types: 1) Thick and sand-rich, lower division (>50 cm-thick) with mud clast layers, and poorly sorted upper division with fine sand component. 2) Thin and silt-rich, lower sandstone division (<20 cm-thick), and poorly sorted upper division, with a minor fine sand component.	Entrainment of mud clasts and fine-grained sediment suppress turbulence and produce high-concentration to pseudo-laminar flows. Bipartite beds form through deposition of the lower division from sand-rich turbidity currents with 'linked' poorly sorted upper division from co-genetic debris flow.	Channel-lobe transition zone, lobe (off-axis, fringe).
Fa21 Debrite	Normally structureless. Can show dewatering structures.	5 mm to several m.	Sharp bases and tops.	From 10s of cm to 10s of m-thick, typically thickening down-dip. Limited by shape of containing scour / bed topography or show lateral extents of many kilometres.	Organic-rich, grey coloured and crumbly weathered. Plant fragments often in large proportion, and rise to top of beds.	High density cohesive flows preserving organic fragments. Reduced friction effects of debris flows riding over de-watered sands deposited by precursor turbidity current.	Channel (axis), delta front, degraded slope, lobe (fringe).

Table 1. Unit G facies classification, description and interpretation of the main processes and environments of deposition. For further information about facies associations see Table 2.

FACIES ASSOCIATION	TYPYCAL LITHOFACIES	MAIN CHARACTERISTICS
Offshore	- Mudstone: structureless mudstone (**Fa1**), structureless to laminated siltstone (**Fa2**)	10's of m-thick fine-grained packages separating coarser-grained units, found above flooding surfaces. Clastic starved background deposition in offshore, basinal settings. Excellent correlation markers, mappable laterally and down-dip throughout the study area. Thicken significantly basinward, to the north and east.
Prodelta	- Mudstone: structureless to laminated siltstone (**Fa2**) - Interbedded: silt-prone (**Fa4**), sand-prone (**Fa5**) - Sandstone: normal (**Fa8**) to inversely-graded (**Fa9**), unidirectional ripple-laminated (**Fa11**)	10's of m-thick coarsening and thickening-up packages of rhythmically interbedded silty mudstones and very fine-grained sandstones. Distal river-dominated deposits. Regionally extensive, sheet to wedge geometry along 100s of m to several km, thicken basinward. Conformably found above offshore mudstones.
Delta front	- Interbedded: sand-prone (**Fa5**) - Sandstone: structureless (**Fa6**), structured (**Fa7**), normal (**Fa8**) to inversely-graded (**Fa9**), parallel-bedded (**Fa10**), unidirectional (**Fa11**) to climbing ripple-laminated (**Fa14**) - Conglomerate: mudclast conglomerate (**Fa17**) - Other: folded and megaclast deposits (**Fa19**), debrite (**Fa21**)	Several m-thick coarsening and thickening-up packages of interbedded to bedded very fine to fine-grained micaceous and organic-rich sandstones, often deformed and occasionally channelized. Proximal river-dominated deposits. Sheet to lenticular geometry along 10s to 100s of m, thin laterally and basinward passing to more marginal and distal interbedded prodeltaic equivalents. Conformably found above prodelta deposits.
Shoreface-Offshore transition (SOT)	- Interbedded: silt-prone (**Fa4**), sand-prone (**Fa5**) - Sandstone: wave ripple-laminated (**Fa12**), combined-flow cross-bedded (**Fa13**)	10's of m-thick rhythmic alternations of thin-bedded sandstones and siltstones reworked by waning, storm and wave-generated oscillatory currents and combined flows. Low and high-concentration flow deposits above storm weather wave base. Regionally extensive, sheet to wedge geometry along 100s of m to several km, thicken basinward. Conformably found above offshore mudstones.
Shoreface	- Sandstone: structured (**Fa7**), normal (**Fa8**) to inversely-graded (**Fa9**), parallel-bedded (**Fa10**), wave ripple-laminated (**Fa12**), combined-flow cross-bedded (**Fa13**) - Conglomerate: mudclast conglomerate (**Fa17**) - Other: folded and megaclast deposits (**Fa19**), debrite (**Fa21**)	Several m-thick amalgamated and medium to thick-bedded low-angle to swaley cross-bedded sandstones. Migration of subaqueous bedforms affected by combined flows, occasionally deformed. Abrupt facies changes occur over short distances. Sheet to lenticular geometry along 10s to 100s of m. Conformably found above SOT deposits.
Channel-fill	- Mudstone: rhythmically bedded siltstone and mudstone (**Fa3**) - Interbedded: silt-prone (**Fa4**), sand-prone (**Fa5**) - Sandstone: structureless (**Fa6**), structured (**Fa7**), normally-graded (**Fa9**), parallel-bedded (**Fa10**), unidirectional (**Fa11**) to climbing ripple-laminated (**Fa14**) - Conglomerate: mudclast conglomerate (**Fa17**) - Other: injectite (**Fa18**), folded and megaclast deposits (**Fa19**), debrite (**Fa21**)	Few m-thick, lens-shape deposits filling concave-up, erosional surfaces. Subaqueous channel deposits. Axial zones with repeated phases of erosion/deposition, with amalgamated structured and structureless sandstones. Gradual thinning and fining laterally away from axis, with thin-bedded sandstone and siltstones. Low angle erosional surfaces through bed truncation and changes in depositional dip. Common asymmetric fills, with sandstones onlapping one margin and axis to marginal transition at the other. Lenticular geometry along 10s of m.
Degraded slope	- Mudstone: spill-over siltstone-prone (**Fa4**) - Interbedded: silt-prone (**Fa4**), sand-prone (**Fa5**) - Sandstone: structureless (**Fa6**), structured (**Fa7**), normally-graded (**Fa8**) - Other: folded and megaclast deposits (**Fa19**), debrite (**Fa21**)	Few m-thick, chaotic and remobilised deposits infilling accommodation from slide scars and topography created by mass-transport deposits (MTDs), and thinner layers interbedded with turbidites. Graded beds when ponded in 3D enclosing topography. Sharp-topped lateral continuous beds indicate filling and overspill of slide scar surfaces.
Lobes	- Interbedded: silt-prone (**Fa4**), sand-prone (**Fa5**) - Sandstone: structureless (**Fa6**), structured (**Fa7**), normally-graded (**Fa9**), parallel-bedded (**Fa10**), unidirectional (**Fa11**) to climbing ripple-laminated (**Fa14**), sigmoidal (**Fa15**) - Conglomerate: mudclast conglomerate (**Fa17**) - Other: hybrid-event bed (**Fa20**), debrite (**Fa21**)	Few m-thick, tabular-shape deposits. Basin-floor lobe deposits. Axial zones with high sand content and bypass features, common scoured bases and amalgamation. Off axis alternating bedded sandstones and thin-bedded siltstones reflecting lobe switching. Fringes with progressive sand reduction with distance. Thin-bedded sandstones and siltstones, with organic-rich hybrid beds. Sheet to lenticular geometry along 100s of m.
Levee	- Interbedded: silt-prone (**Fa4**), sand-prone (**Fa5**) - Sandstone: sigmoidal (**Fa15**)	10's of m-thick fining and thinning-upward rhythmic alternations of thin-bedded sandstones and siltstones. Levee / overbank deposits reflecting proximity as well as increasing confinement and channel switching/avulsion. Sandstone content decreases non-linearly away from channel. Wedge geometry along 100s of m to several km, thin basinward.

Table 2. Facies associations of Unit G, with the typical lithofacies found, and a summary of the main characteristics. Same colour code as in Fig. 4.

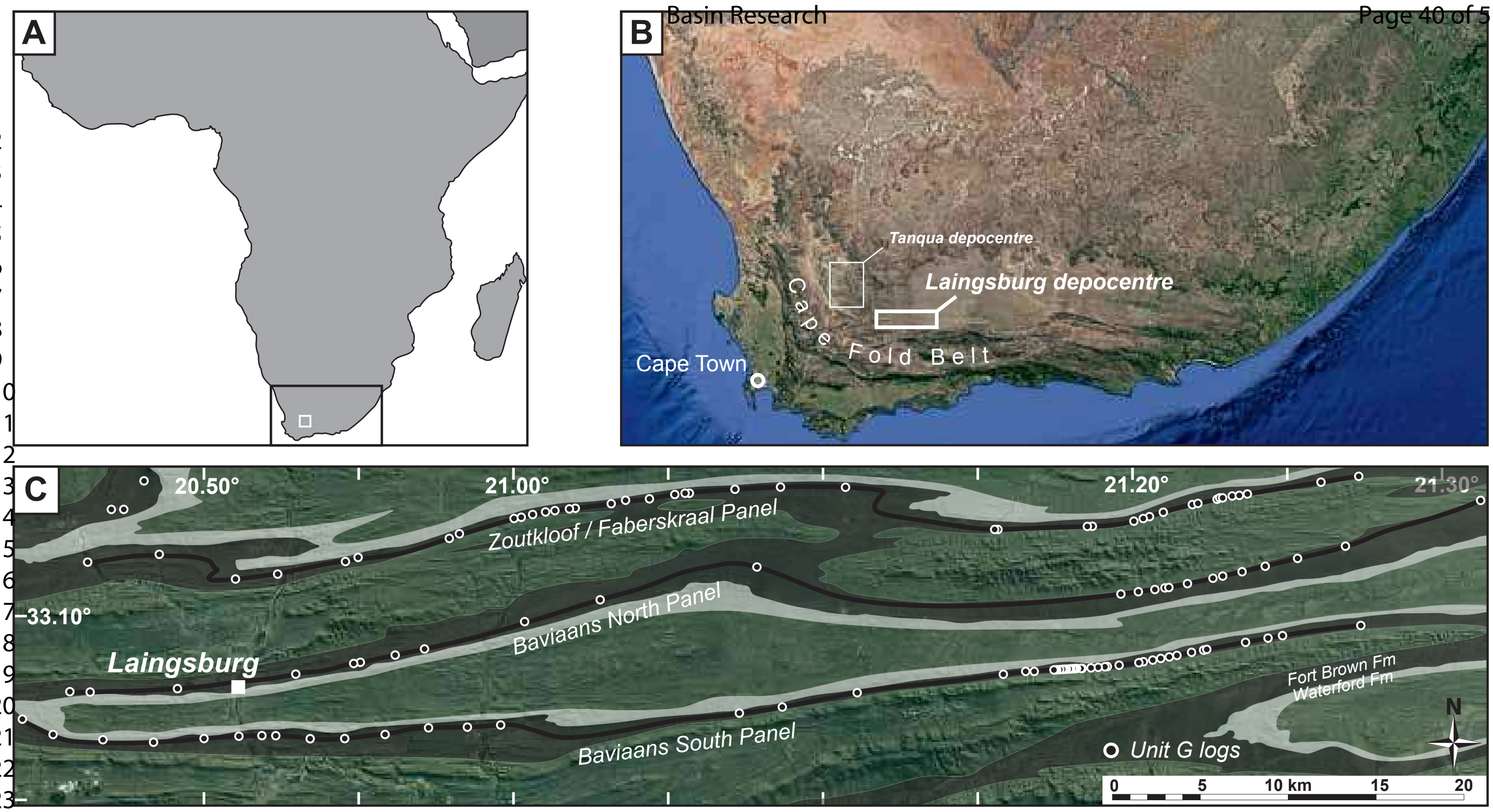
A
B
Tanqua depocentre
Laingsburg depocentre
Cape Fold Belt
Cape Town
C
20.50°
21.00°
21.20°
21.30°
-33.10°
Zoutkloof / Faberskraal Panel
Baviaans North Panel
Laingsburg
Baviaans South Panel
Fort Brown Fm
Waterford Fm
Unit G logs
N
0 5 10 km 15 20

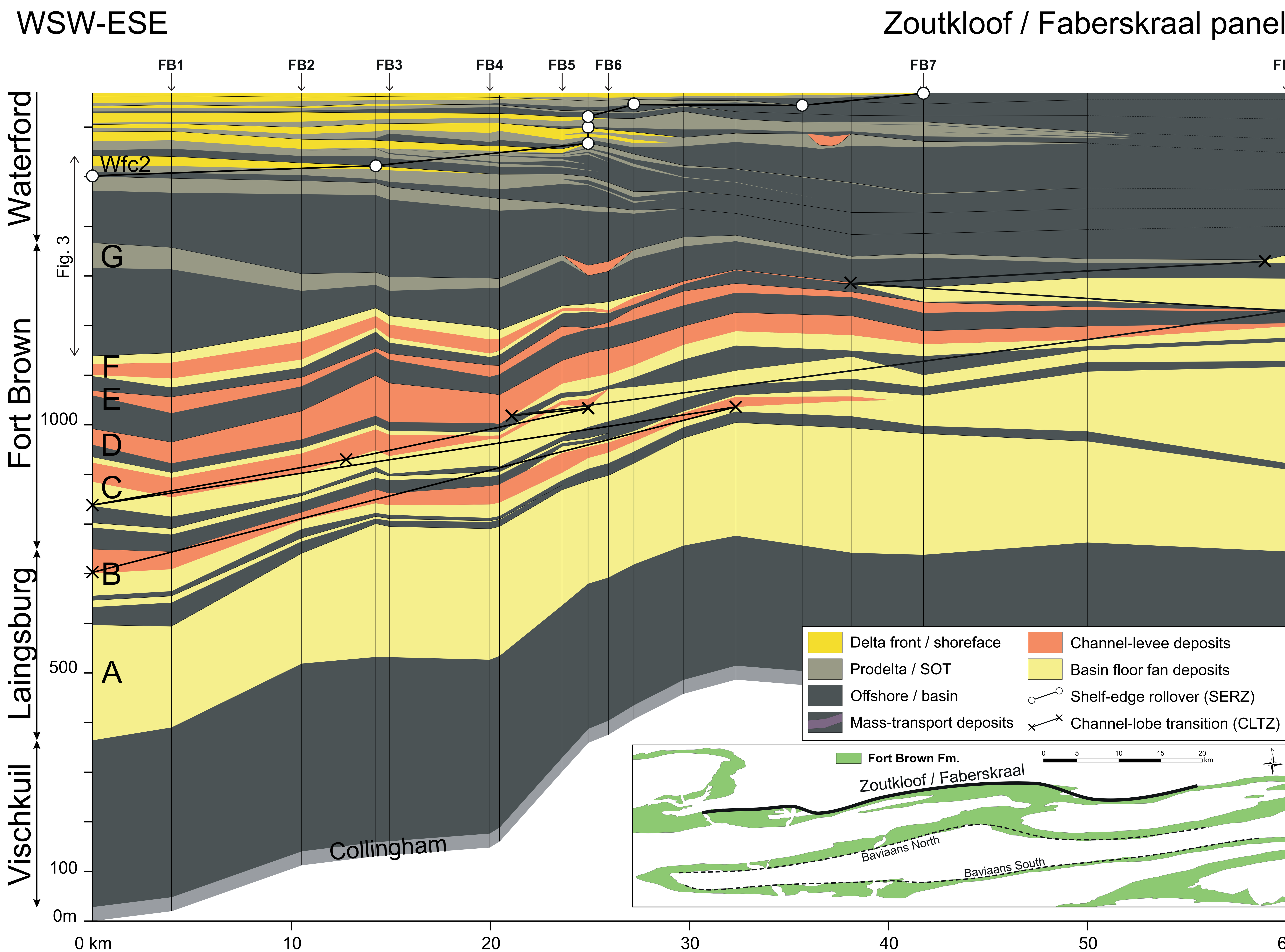
WSW-ESE
Zoutkloof / Faberskraal panel
FB1
FB2
FB3
FB4
FB5
FB6
FB7
FB8
Waterford
Fort Brown
Laingsburg
Vischkuil
Fig. 3
Wfc2
G
F
E
D
C
B
A
Collingham
1000
500
100
0m
0 km
10
20
30
40
50
60
Delta front / shoreface
Prodelta / SOT
Offshore / basin
Mass-transport deposits
Channel-levee deposits
Basin floor fan deposits
Shelf-edge rollover (SERZ)
Channel-lobe transition (CLTZ)
Fort Brown Fm.
Zoutkloof / Faberskraal
Baviaans North
Baviaans South

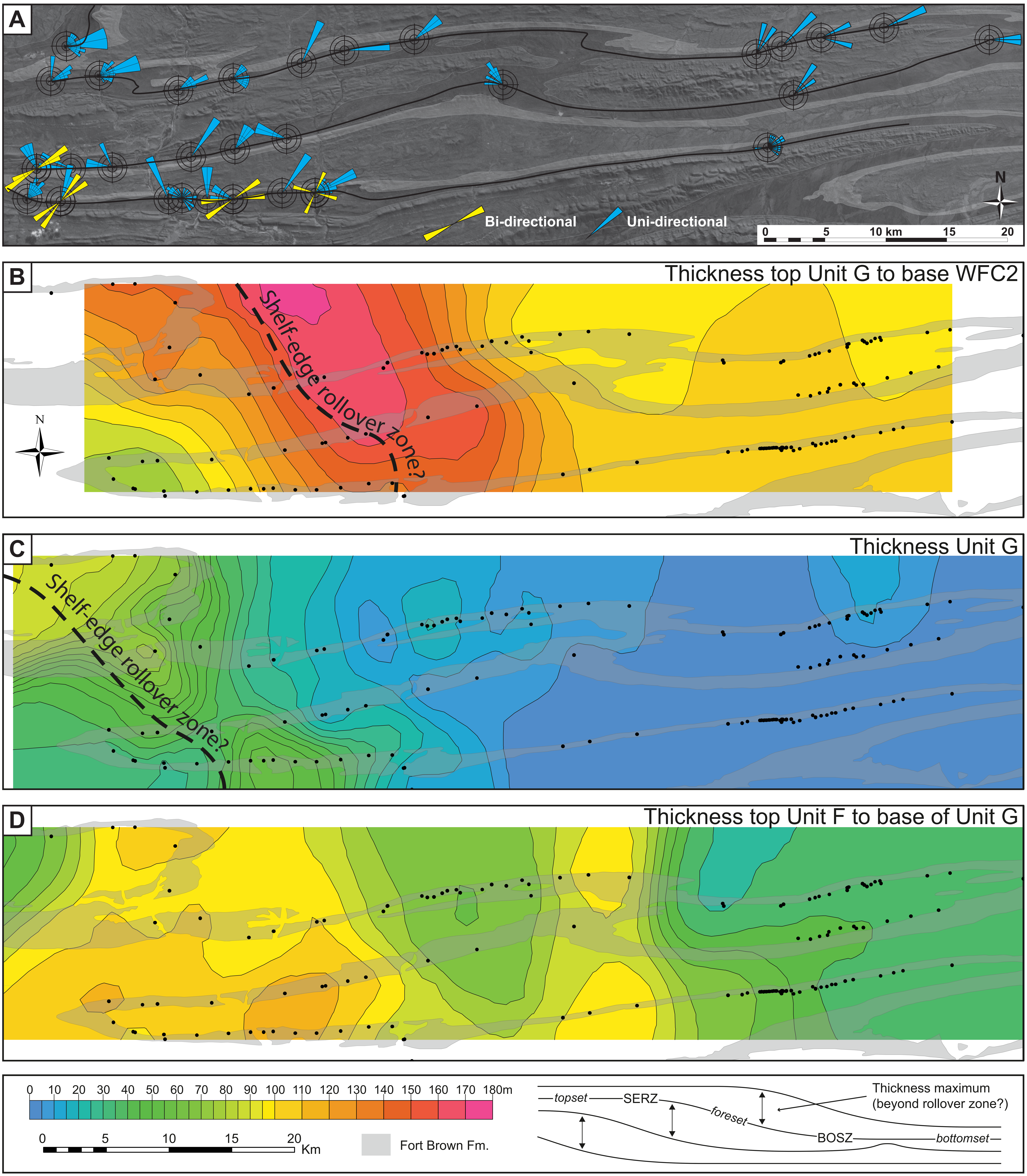
A
Bi-directional
Uni-directional
0 5 10 km 15 20
N
B
Thickness top Unit G to base WFC2
Shelf-edge rollover zone?
N
C
Thickness Unit G
Shelf-edge rollover zone?
D
Thickness top Unit F to base of Unit G
0 10 20 30 40 50 60 70 80 90 100 110 120 130 140 150 160 170 180m
0 5 10 15 20 Km
Fort Brown Fm.
topset
SERZ
foreset
BOSZ
bottomset
Thickness maximum (beyond rollover zone?)

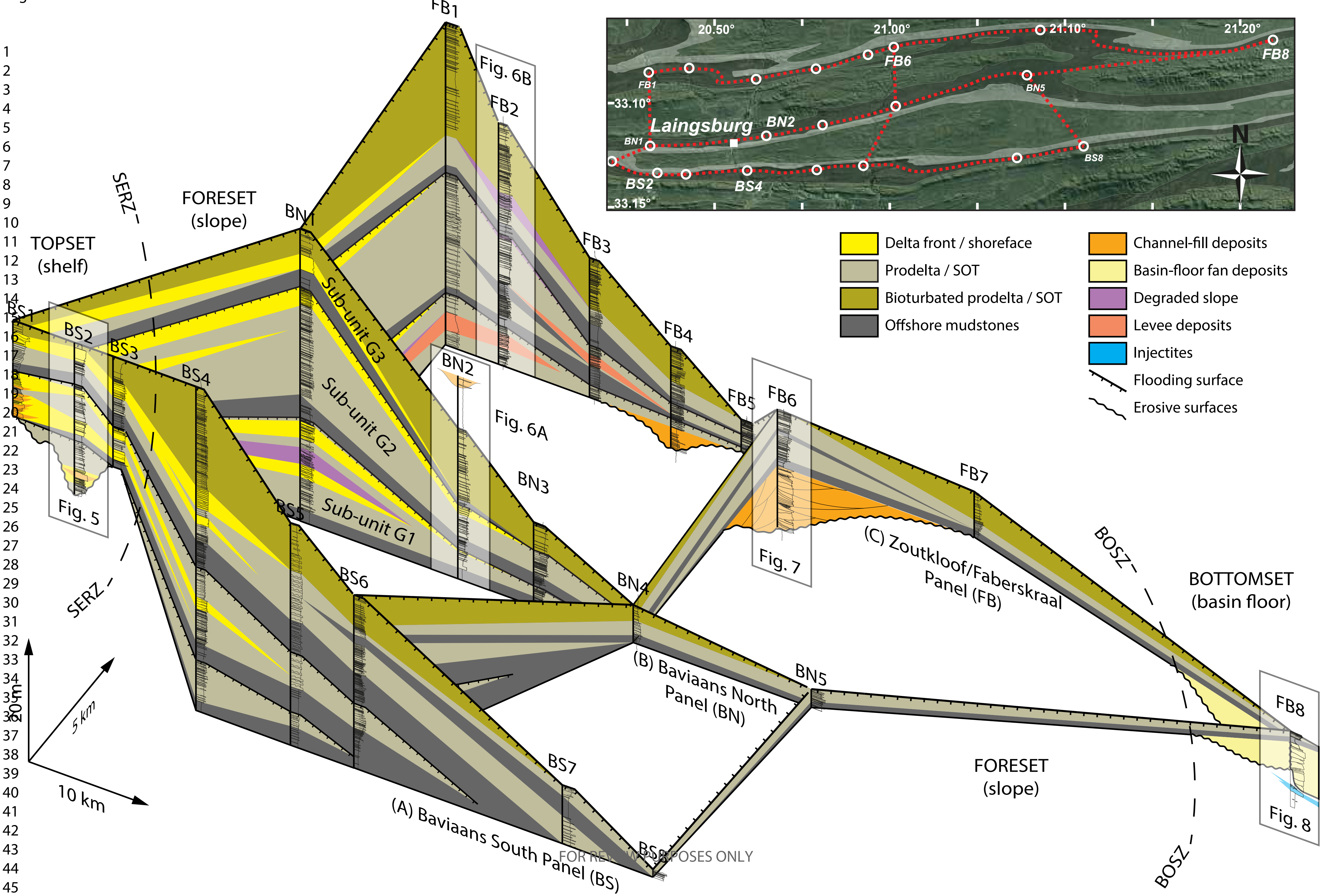

20.50°
21.00°
21.10°
21.20°
-33.10°
-33.15°
Laingsburg
FB1
FB6
FB8
BN1
BN2
BN5
BS2
BS4
BS8
N
Delta front / shoreface
Prodelta / SOT
Bioturbated prodelta / SOT
Offshore mudstones
Channel-fill deposits
Basin-floor fan deposits
Degraded slope
Levee deposits
Injectites
Flooding surface
Erosive surfaces
TOPSET
(shelf)
FORESET
(slope)
BOTTOMSET
(basin floor)
SERZ
BOSZ
FB1
FB2
FB3
FB4
FB5
FB6
FB7
FB8
BN1
BN2
BN3
BN4
BN5
BS1
BS2
BS3
BS4
BS5
BS6
BS7
BS8
Fig. 5
Fig. 6A
Fig. 6B
Fig. 7
Fig. 8
Sub-unit G3
Sub-unit G2
Sub-unit G1
(A) Baviaans South Panel (BS)
(B) Baviaans North Panel (BN)
(C) Zoutkloof/Faberskraal Panel (FB)
20 m
5 km
10 km

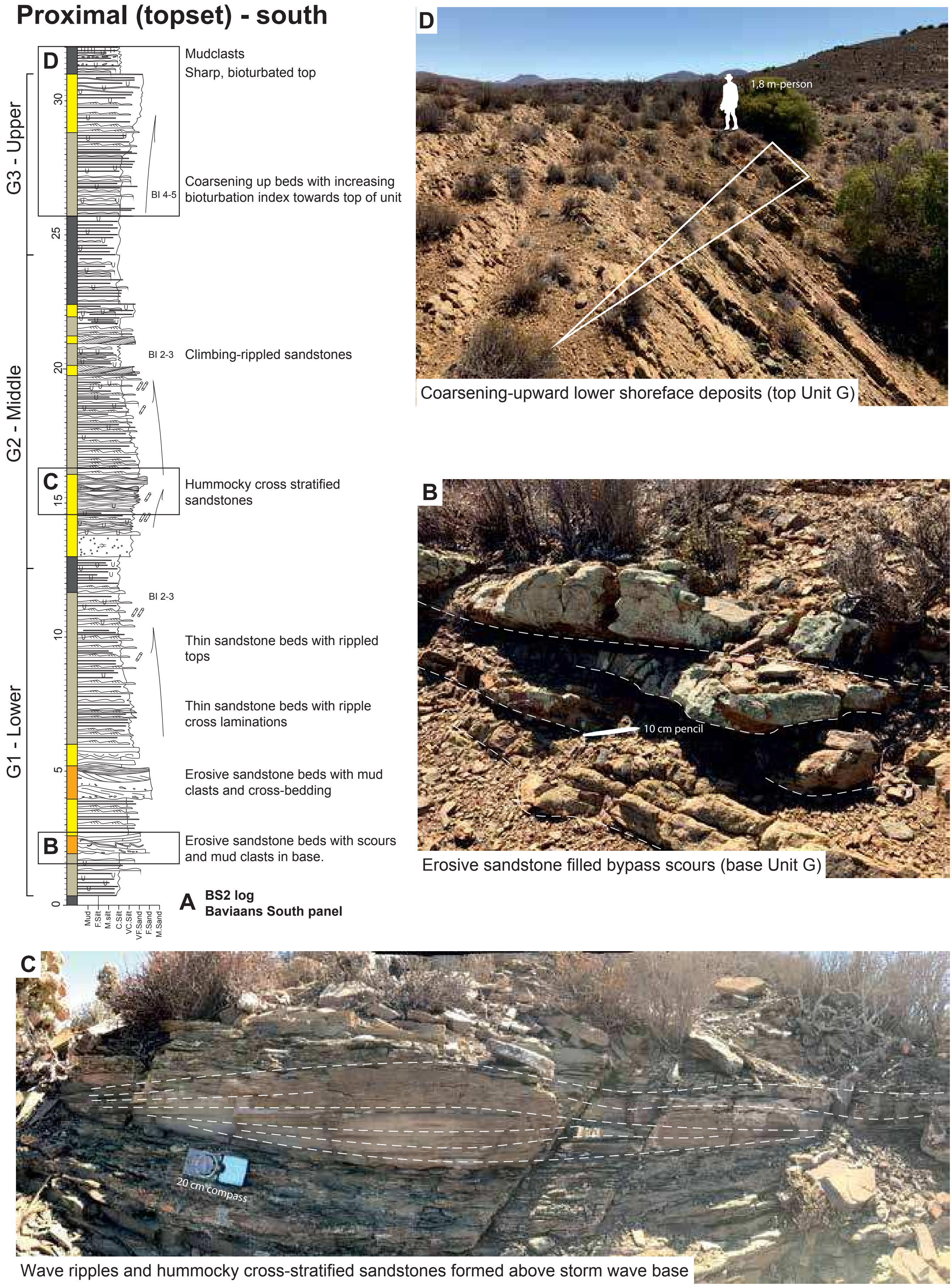
Proximal (topset) - south
D
C
B
A
BS2 log
Baviaans South panel
G3 - Upper
G2 - Middle
G1 - Lower
Mudclasts
Sharp, bioturbated top
Coarsening up beds with increasing bioturbation index towards top of unit
BI 4-5
BI 2-3
Climbing-rippled sandstones
Hummocky cross stratified sandstones
BI 2-3
Thin sandstone beds with rippled tops
Thin sandstone beds with ripple cross laminations
Erosive sandstone beds with mud clasts and cross-bedding
Erosive sandstone beds with scours and mud clasts in base.
0
5
10
15
20
25
30
Mud
F.Silt
M.silt
C.Silt
VC.Silt
VF.Sand
F.Sand
M.Sand
1,8 m-person
Coarsening-upward lower shoreface deposits (top Unit G)
10 cm pencil
Erosive sandstone filled bypass scours (base Unit G)
20 cm compass
Wave ripples and hummocky cross-stratified sandstones formed above storm wave base

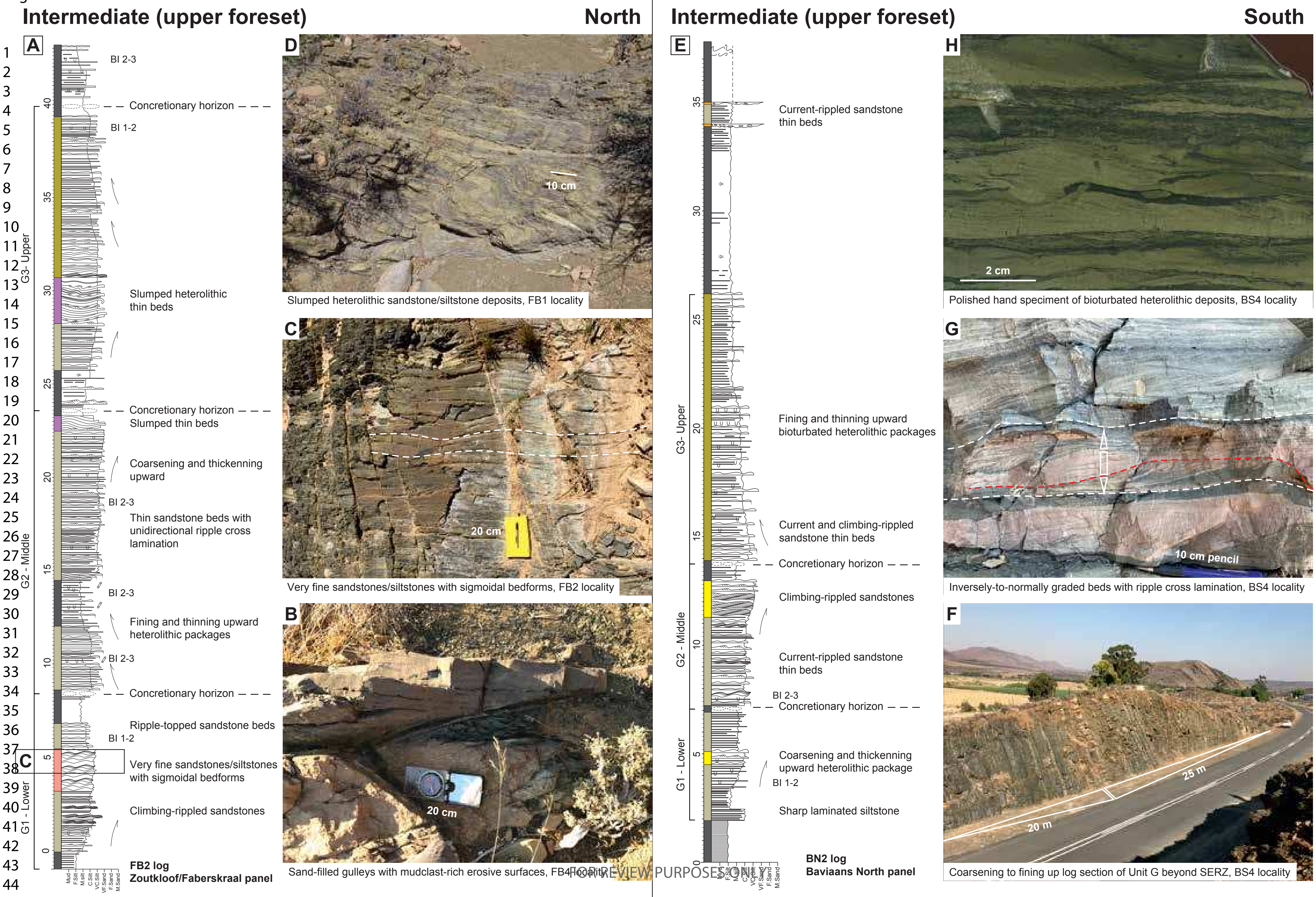
Intermediate (upper foreset)
North
Intermediate (upper foreset)
South
A
BI 2-3
Concretionary horizon
BI 1-2
Slumped heterolithic thin beds
Concretionary horizon
Slumped thin beds
Coarsening and thickenning upward
BI 2-3
Thin sandstone beds with unidirectional ripple cross lamination
BI 2-3
Fining and thinning upward heterolithic packages
BI 2-3
Concretionary horizon
Ripple-topped sandstone beds
BI 1-2
C
Very fine sandstones/siltstones with sigmoidal bedforms
Climbing-rippled sandstones
G3- Upper
G2 - Middle
G1 - Lower
Mud
F.Silt
M.Silt
C.Silt
VC.Silt
VF.Sand
F.Sand
M.Sand
FB2 log
Zoutkloof/Faberskraal panel
D
10 cm
Slumped heterolithic sandstone/siltstone deposits, FB1 locality
C
20 cm
Very fine sandstones/siltstones with sigmoidal bedforms, FB2 locality
B
20 cm
Sand-filled gulleys with mudclast-rich erosive surfaces, FB4 locality
E
Current-rippled sandstone thin beds
Fining and thinning upward bioturbated heterolithic packages
Current and climbing-rippled sandstone thin beds
Concretionary horizon
Climbing-rippled sandstones
Current-rippled sandstone thin beds
BI 2-3
Concretionary horizon
Coarsening and thickenning upward heterolithic package
BI 1-2
Sharp laminated siltstone
G3- Upper
G2 - Middle
G1 - Lower
BN2 log
Baviaans North panel
H
2 cm
Polished hand specimen of bioturbated heterolithic deposits, BS4 locality
G
10 cm pencil
Inversely-to-normally graded beds with ripple cross lamination, BS4 locality
F
25 m
20 m
Coarsening to fining up log section of Unit G beyond SERZ, BS4 locality

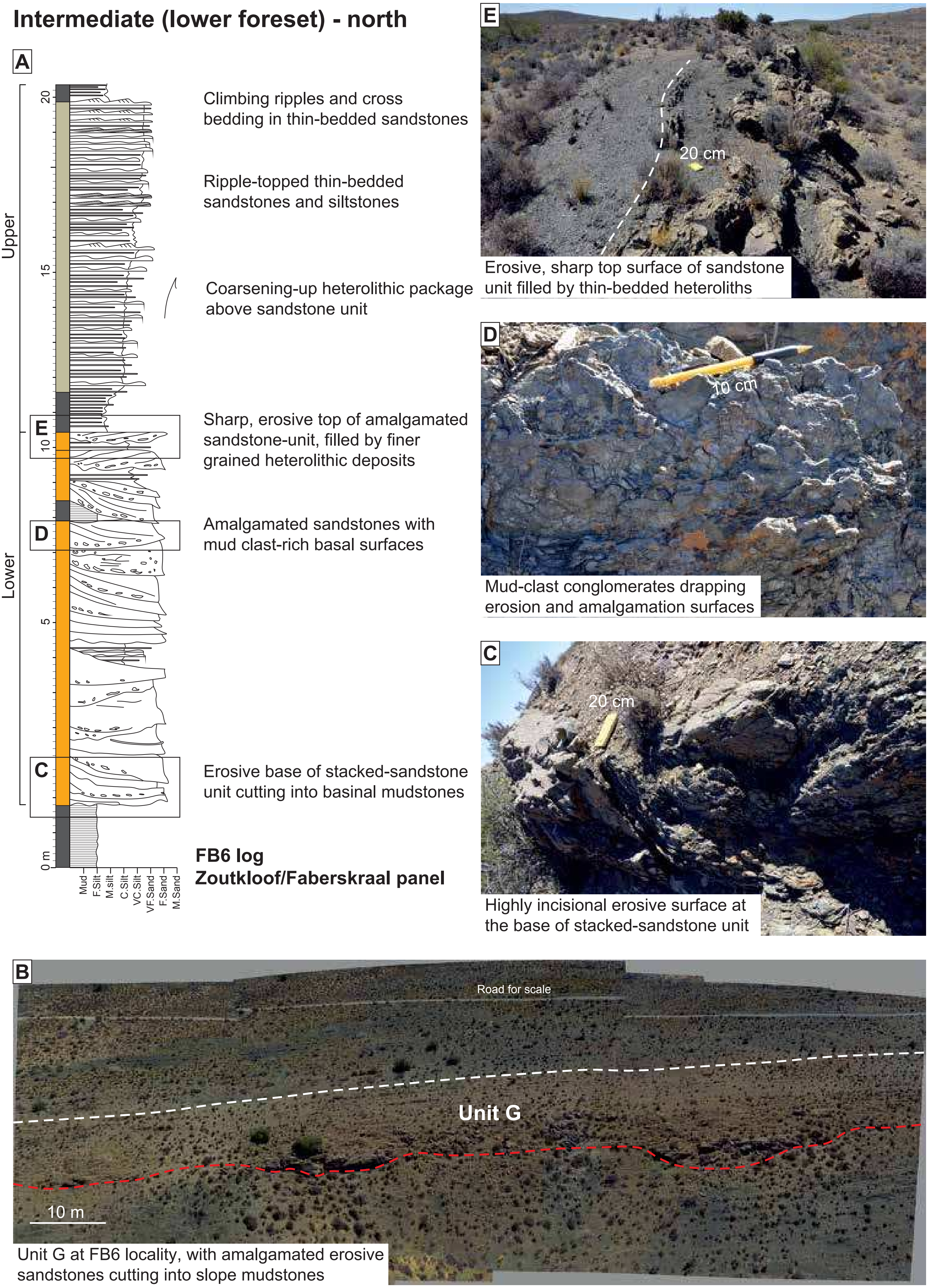
Intermediate (lower foreset) - north
A
Upper
Lower
20
15
10
5
0 m
Mud
F.Silt
M.silt
C.Silt
VC.Silt
VF.Sand
F.Sand
M.Sand
E
D
C
Climbing ripples and cross bedding in thin-bedded sandstones
Ripple-topped thin-bedded sandstones and siltstones
Coarsening-up heterolithic package above sandstone unit
Sharp, erosive top of amalgamated sandstone-unit, filled by finer grained heterolithic deposits
Amalgamated sandstones with mud clast-rich basal surfaces
Erosive base of stacked-sandstone unit cutting into basinal mudstones
FB6 log
Zoutkloof/Faberskraal panel
E
20 cm
Erosive, sharp top surface of sandstone unit filled by thin-bedded heteroliths
D
10 cm
Mud-clast conglomerates drapping erosion and amalgamation surfaces
C
20 cm
Highly incisional erosive surface at the base of stacked-sandstone unit
B
Road for scale
Unit G
10 m
Unit G at FB6 locality, with amalgamated erosive sandstones cutting into slope mudstones

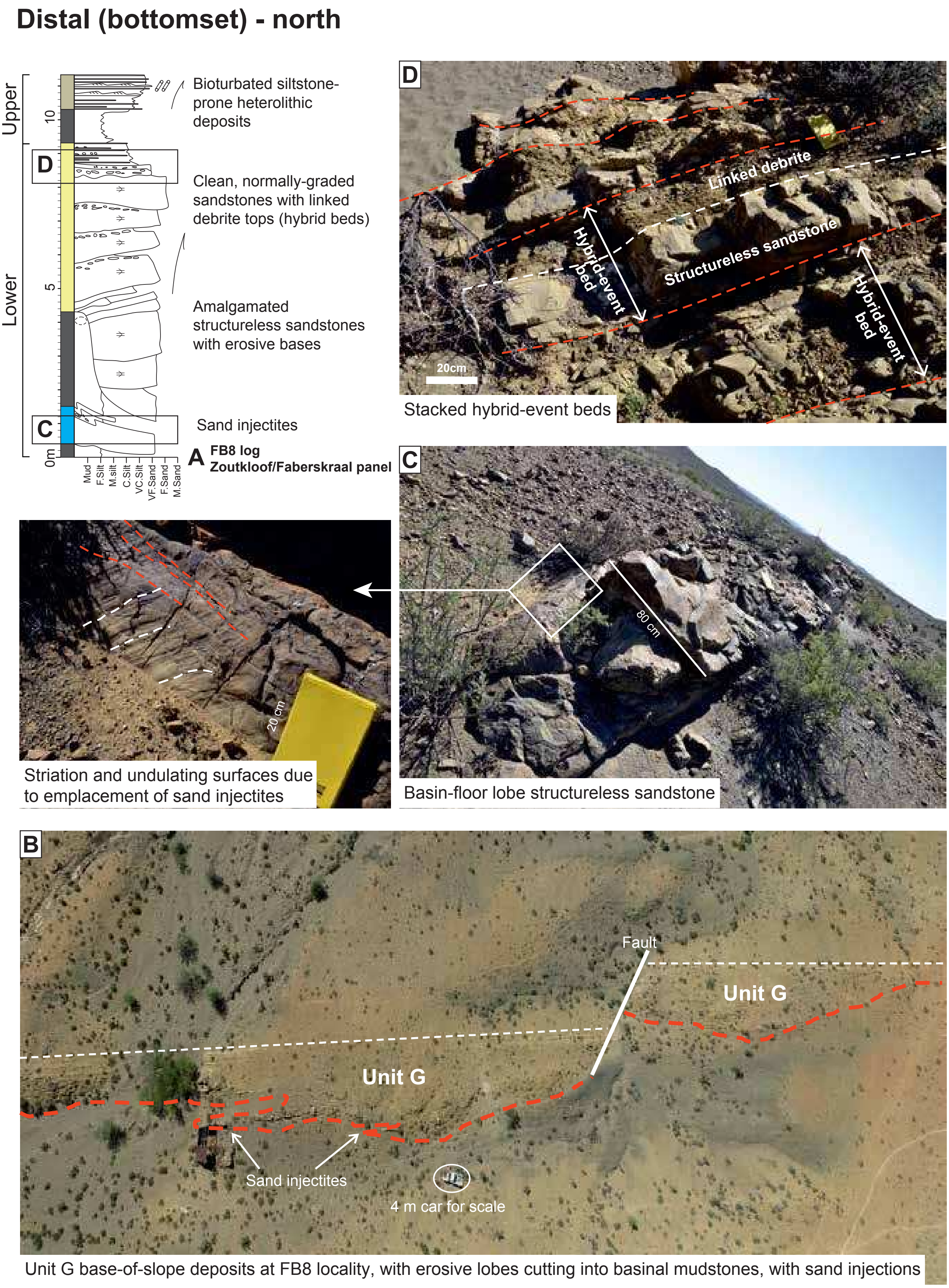
Distal (bottomset) - north
Upper
Lower
10
5
0m
D
C
Bioturbated siltstone-prone heterolithic deposits
Clean, normally-graded sandstones with linked debrite tops (hybrid beds)
Amalgamated structureless sandstones with erosive bases
Sand injectites
A FB8 log Zoutkloof/Faberskraal panel
Mud
F.Silt
M.silt
C.Silt
VC.Silt
VF.Sand
F.Sand
M.Sand
Linked debrite
Hybrid-event bed
Structureless sandstone
Hybrid-event bed
20cm
Stacked hybrid-event beds
80 cm
20 cm
Striation and undulating surfaces due to emplacement of sand injectites
Basin-floor lobe structureless sandstone
B
Fault
Unit G
Unit G
Sand injectites
4 m car for scale
Unit G base-of-slope deposits at FB8 locality, with erosive lobes cutting into basinal mudstones, with sand injections

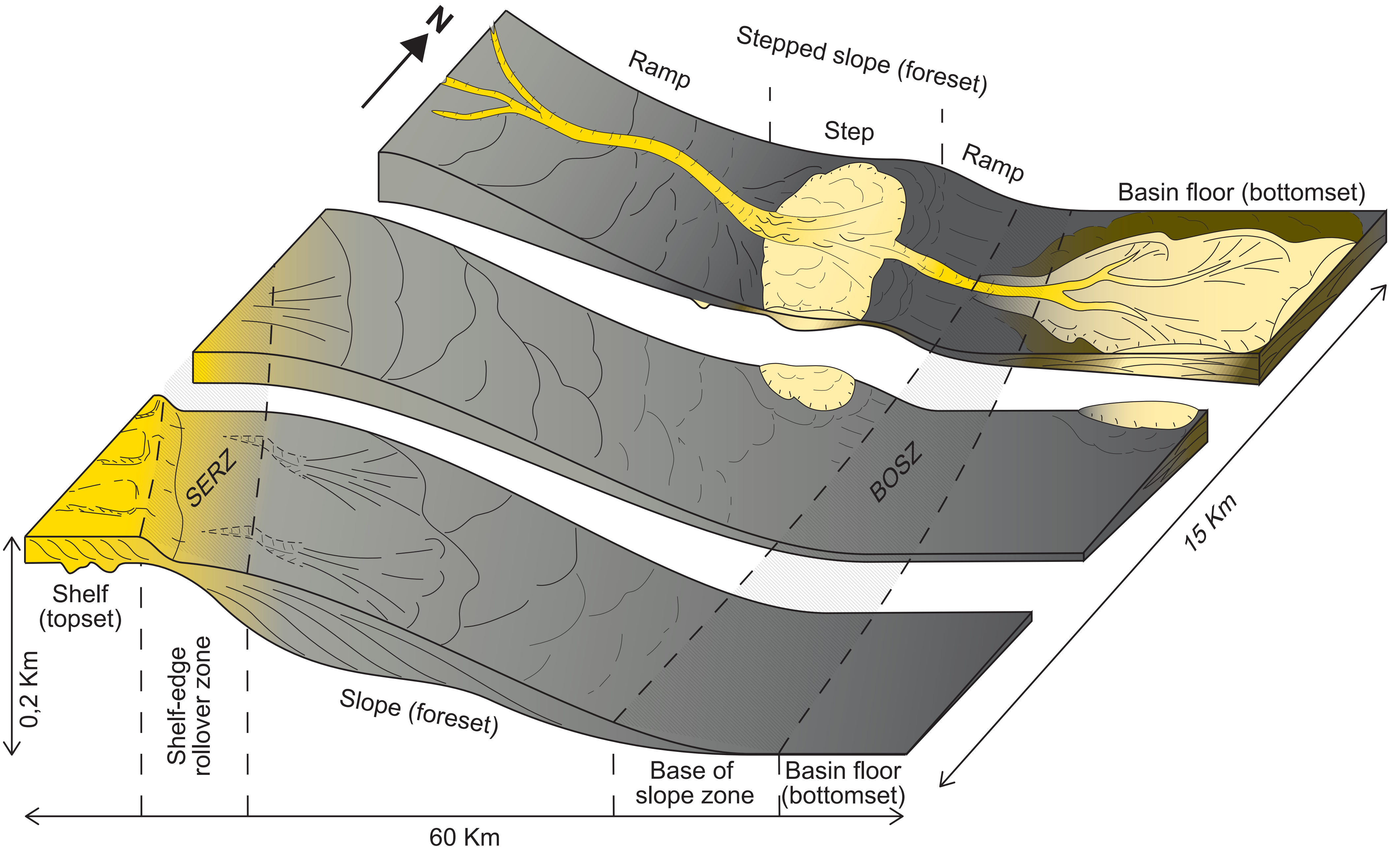
N
Ramp
Stepped slope (foreset)
Step
Ramp
Basin floor (bottomset)
SERZ
BOSZ
15 Km
0,2 Km
Shelf
(topset)
Shelf-edge
rollover zone
Slope (foreset)
Base of
slope zone
Basin floor
(bottomset)
60 Km

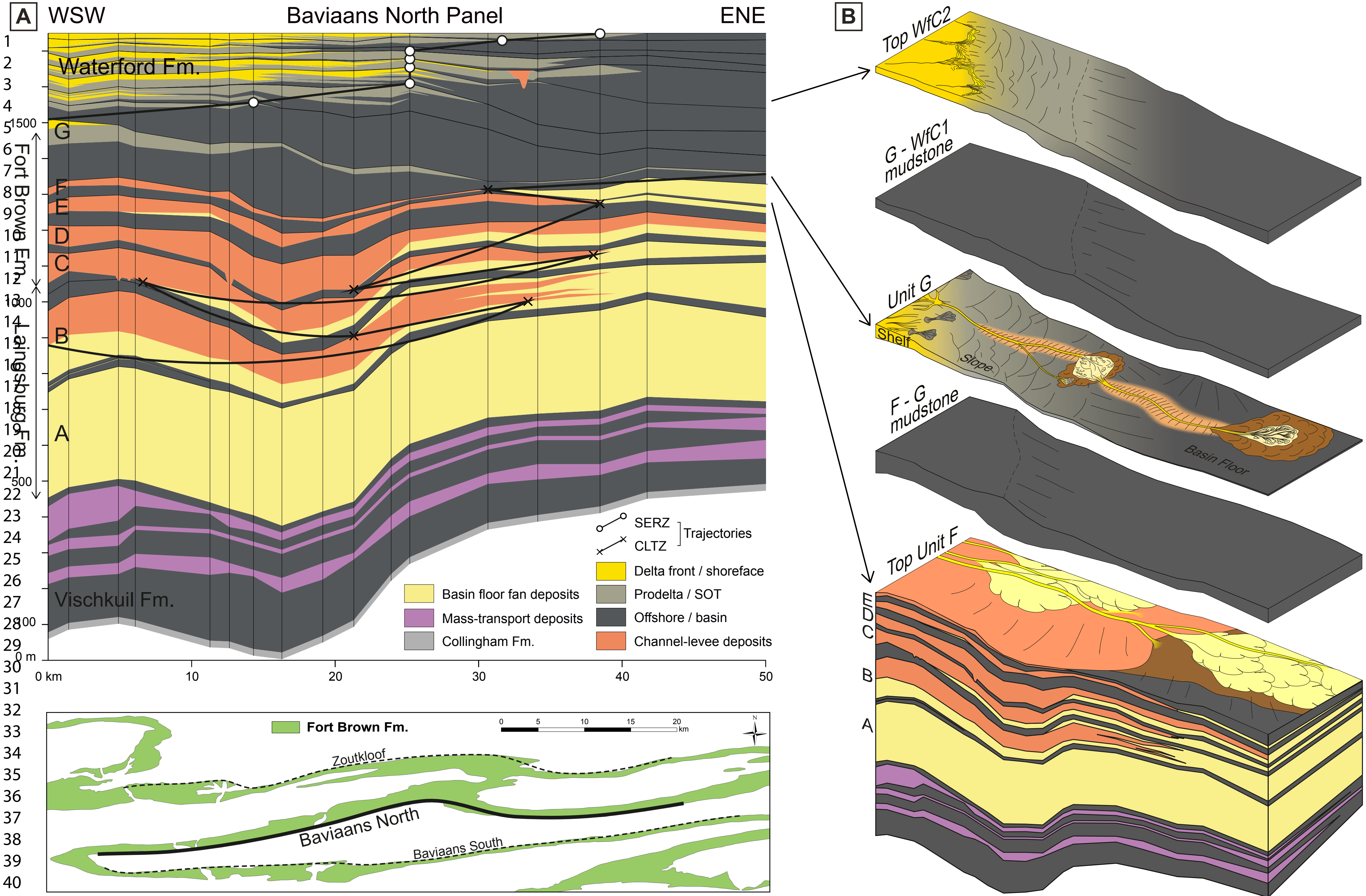
A
WSW
Baviaans North Panel
ENE
Waterford Fm.
G
F
E
D
C
B
A
Fort Brown Fm.
Laingsburg Fm.
Vischkuil Fm.
1500
1000
500
0 m
0 km
10
20
30
40
50
SERZ
CLTZ
Trajectories
Delta front / shoreface
Prodelta / SOT
Offshore / basin
Channel-levee deposits
Basin floor fan deposits
Mass-transport deposits
Collingham Fm.
Fort Brown Fm.
0
5
10
15
20
km
N
Zoutkloof
Baviaans North
Baviaans South
B
Top WfC2
G - WfC1 mudstone
Unit G
Shelf
Slope
Basin Floor
F - G mudstone
Top Unit F
E
D
C
B
A

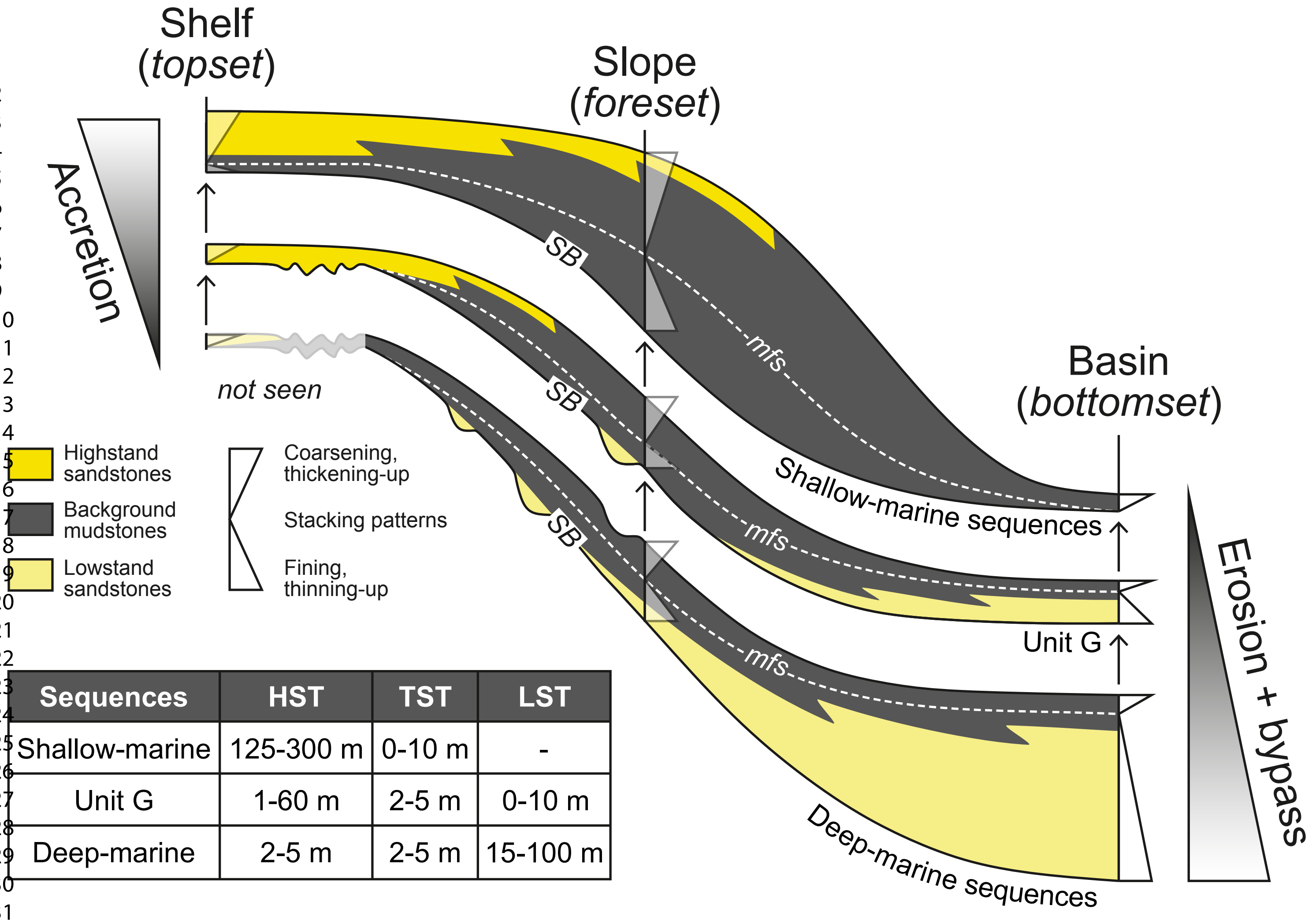

Sequences	HST	TST	LST
Shallow-marine	125-300 m	0-10 m	-
Unit G	1-60 m	2-5 m	0-10 m
Deep-marine	2-5 m	2-5 m	15-100 m

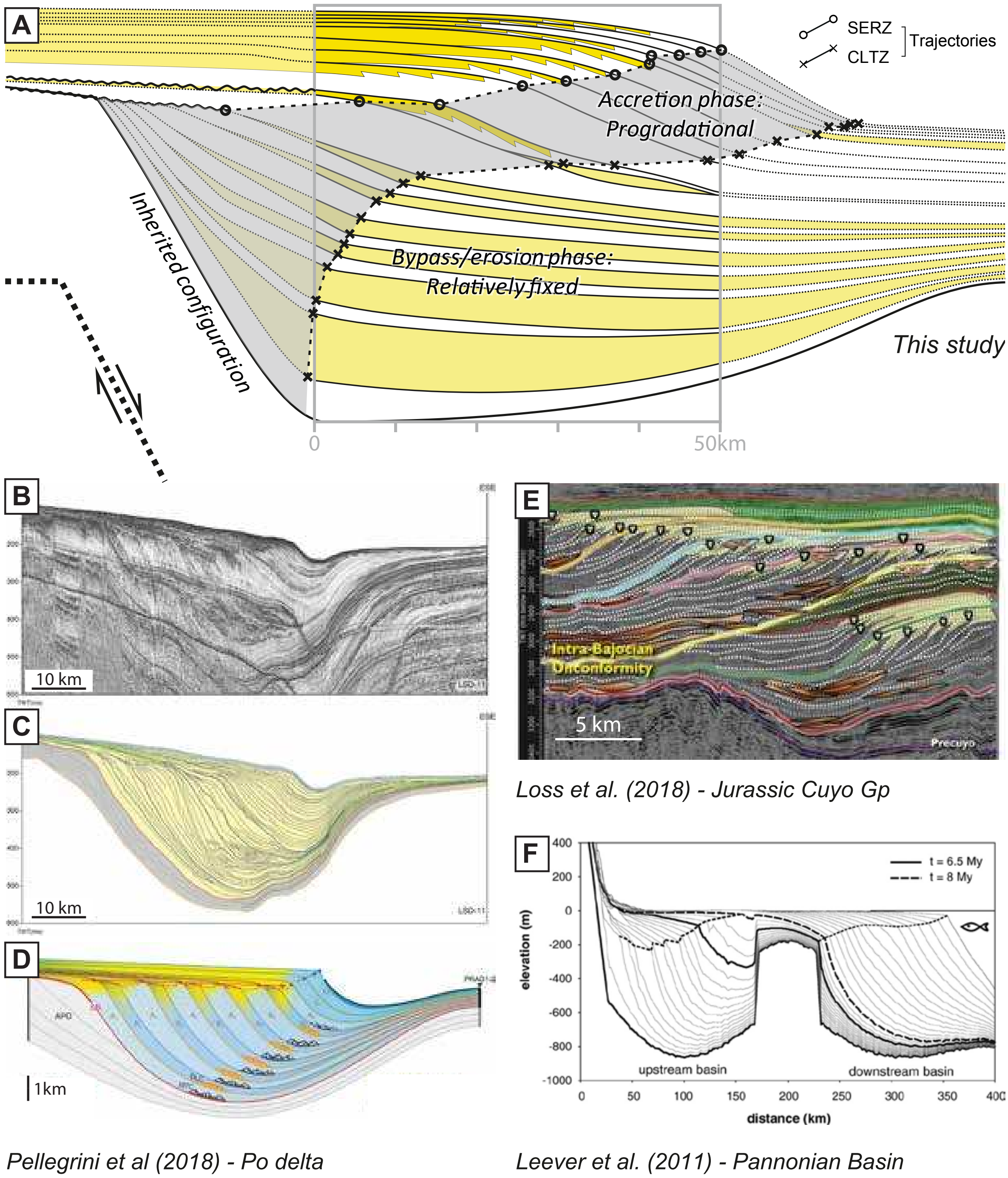
A
SERZ
CLTZ
Trajectories
Accretion phase:
Progradational
Bypass/erosion phase:
Relatively fixed
Inherited configuration
This study
0
50km
B
10 km
C
10 km
D
1km
Pellegrini et al (2018) - Po delta
E
Intra-Bajocian
Unconformity
5 km
Precuyo
Loss et al. (2018) - Jurassic Cuyo Gp
F
t = 6.5 My
t = 8 My
elevation (m)
upstream basin
downstream basin
distance (km)
Leever et al. (2011) - Pannonian Basin